Ph.D. DISSERTATION

Effects of Charge Balance on Device Performances of Solution Processed QLEDs

용액 공정 기반의 양자점 발광 다이오드 : 전하 균형이 소자 특성에 미치는 영향

AUGUST 2023

DEPARTMENT OF ELECTRICAL
AND COMPUTER ENGINEERING
COLLEGE OF ENGINEERING
SEOUL NATIONAL UNIVERSITY

YISEUL KIM

Effects of Charge Balance on Device Performances of Solution Processed QLEDs

용액 공정 기반의 양자점 발광 다이오드 : 전하 균형이 소자 특성에 미치는 영향

지도교수 홍 용 택

이 논문을 공학박사 학위논문으로 제출함
2023 년 8 월

서울대학교 대학원
전기 · 정보 공학부
김 이 슬

김이슬의 공학박사 학위논문을 인준함
2023 년 8 월

위 원 장 정 윤 찬 (인)
부위원장 홍 용 택 (인)
위 원 곽 정 훈 (인)
위 원 유 승 협 (인)
위 원 진 병 두 (인)

Abstract

Effects of Charge Balance on Device Performances of Solution Processed QLEDs

YISEUL KIM
DEPARTMENT OF ELECTRICAL AND COMPUTER ENGINEERING
COLLEGE OF ENGINEERING
SEOUL NATIONAL UNIVERSITY

As the application of display technology becomes increasingly diversified and advanced, related technologies continue to evolve to meet a wide range of demands. Following the decline of display technologies like cathode ray tube (CRT) and liquid crystal display (LCD), which relied on backlight units as a crucial component, the market has been dominated by displays based on active matrix light emitting diodes (LED and Organic LED). Recently, quantum dots (QDs) and perovskite have emerged as highly promising next-generation materials in the field of displays. Particularly, QDs are semiconductor materials renowned for their outstanding electrical and optical properties, enabling their utilization in various products such as light-emitting devices and sensors. Moreover, they offer the advantage of easily adjusting the emission/absorption wavelength through particle size control, resulting in remarkable color purity and brightness. Furthermore,

characteristics of QDs can be tailored in multiple ways by manipulating the core-shell/ligand configuration. Additionally, QDs can be employed in solvent-dispersed form, allowing for cost-effective and low-temperature processing through solution-based methods. Consequently, QDs are receiving increasing attention for their potential application in large-area, flexible, and stretchable electronic devices.

The most efficient and straightforward technique employed for the fabrication of quantum dot light emitting diodes (QLEDs) is widely known as spin coating. Spin coating involves depositing thin films onto a rotating substrate by dispensing a solution onto it, utilizing the centrifugal force generated by rotation. This method offers a simple process with rapid coating speed, facilitating the production of films with relatively uniform thickness. Furthermore, spin coating provides the advantage of easy control over the film thickness by adjusting parameters such as rotation speed, duration, and solution concentration.

However, QLEDs produced through this method exhibit a limitation in their intrinsic characteristics, specifically in a charge imbalance state caused by the deep valence band maximum (VBM) of the QDs. Due to the deep VBM of QDs, the hole injection barrier is significantly larger compared to the electron injection barrier into the emitting layer (EML). Additionally, hole mobility in hole transport layers (HTL), which can be achieved using a solution process, is known to be significantly lower than the electron mobility in electron transport layers (ETL). Consequently, hole injection is disadvantaged in terms of both injection barrier and carrier mobility when compared to electron injection. As a result, an excess of electrons leads to a charge imbalance state. This charge imbalance induces non-radiative

recombination, a significant factor that deteriorates device performance. To address these issues, this paper presents a range of strategies for developing alternative device structures.

Initially, we introduced a novel device structure that involves the incorporation of monomers within the HTL without the addition of an active layer. Unlike QLEDs employing an inverted structure, where a deposition process is employed to enhance hole injection via a hole injection layer, our proposed structure offers the advantage of regulating hole mobility and injection barriers by incorporating monomers. This approach enables us to retain the existing structure and process while achieving control over hole injection. To realize this device structure, we conducted an extensive search for monomers possessing suitable properties and conducted a preliminary assessment of solubility and solvent compatibility. As a result, we achieved effective enhancement of hole injection while maintaining a simplified process, leading to significant improvements in the optical and electrical properties of the device.

Subsequently, our objective was to devise a device structure capable of mitigating the abundance of excess electrons. To achieve this, we explored two approaches: incorporating an electron injection barrier to suppress excess electrons and controlling the electron mobility within the ETL. Additionally, we conducted an investigation into the underlying principles governing the behavior of the device as the excess electrons were regulated. Through this study, we successfully alleviated the charge imbalance state, leading to the development of a highly reliable device structure.

The primary focus of this dissertation was to establish a process technology that enables the application of diverse monomers in a solution-

based approach and establish a foundational technology for enhancing the performance of QLEDs. Particularly, our aim was to optimize the characteristics of QLEDs by leveraging the unique properties of the monomers, thus enabling tailored improvements in power consumption, efficiency, and stability. By presenting a comprehensive QLED development strategy, we anticipated that this work would contribute significantly to the advancement of foundational technologies facilitating the integration of QLEDs within the display industry.

Keyword: Solution-process, Quantum Dots, Quantum Dot Light Emitting Diodes, Monomer, Charge balance

Student Number: 2019-30461

Table of Contents

List of Tables

List of Figures

Chapter 1

Introduction

1.1 Quantum Dots (QDs)

Quantum dots (QDs) are semiconductor nanocrystals with a size of 10 nm or smaller, possessing a distinct bandgap. Notably, QDs exhibit both photoluminescence (PL) and electroluminescence (EL), making them highly suitable as light-emitting materials. Leveraging QDs in lighting applications enables the attainment of exceptional color purity and luminance. Additionally, the emission/absorption wavelength of QDs can be easily adjusted by manipulating the particle size, allowing for tailored optimization based on specific requirements **(Figure 1.1)** [1-4]. QDs also offer process advantages, as they can be fabricated through all-solution processes, facilitating the realization of flexible devices through layer stacking on flexible substrates. Consequently, the potential applications of QDs are virtually limitless, and their versatility has garnered attention across various fields [5-8].

In the field of bio-imaging, QDs are actively researched due to their compact size and luminous characteristics. First of all, QDs are widely studied in the field of bio-imaging [9, 10]. Moreover, QDs are investigated for energy harvesting applications, such as in solar cells [11], owing to their broad absorption band. Additionally, QDs are attracting interest as catalysts

for CO_2 decomposition [12]. Notably, QDs possess a narrow emission spectrum compared to other light-emitting materials, making them valuable for laser applications [13] and as image sensors [14]. Consequently, QDs find diverse applications. However, the field that particularly leverages the outstanding optical properties of QDs is the display industry [15].

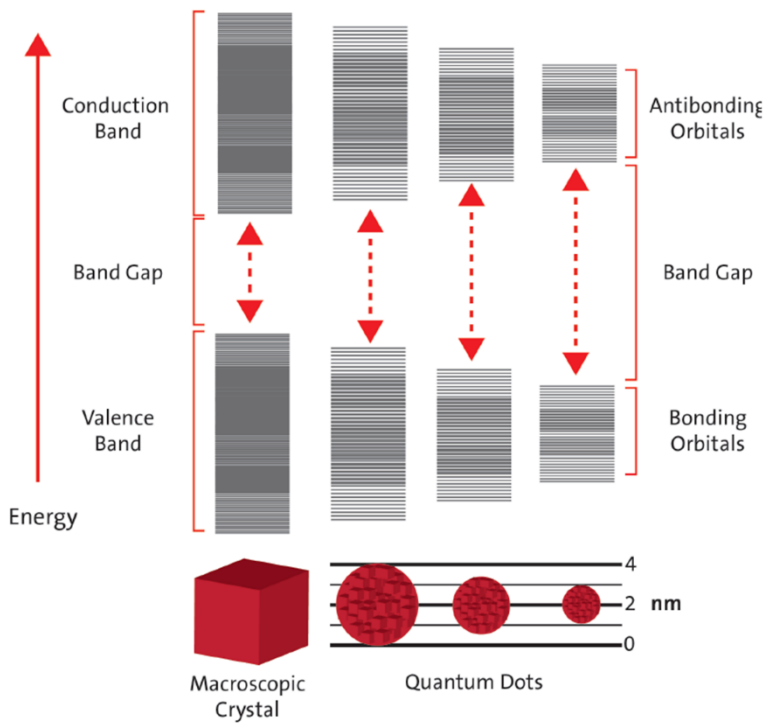

Figure 1.1. Discrete energy levels and sizes of the quantum dots. (source: Quantum Dots and Their Potential Impact on Lighting and Display Applications, 2017)

1.2 Quantum Dots in Displays

The utilization of quantum dots (QDs) in the field of displays encompasses diverse approaches. Firstly, in QD-enhanced film LCDs, a yellow QD film is created by combining red and green QDs, which absorbs a portion of the blue backlight to achieve a white color **(Figure 1.2(a))**. Secondly, QD-OLED employs a similar blue backlight strategy **(Figure 1.2(b))**, but instead of mixing red and green QDs, each color is separately applied as a distinct color conversion layer to realize red, green, and blue pixels. While both these methods harness the photoluminescence (PL) of QDs, the final method, referred to as the QLED method, leverages the electroluminescence (EL) of QDs within a multi-layered device **(Figure 1.2(c))**. The QLED method exhibits the most promising implementation potential as it maximizes the unique characteristics of QDs as semiconducting materials, enables the construction of thin panels without components like color filters, and facilitates flexible display applications.

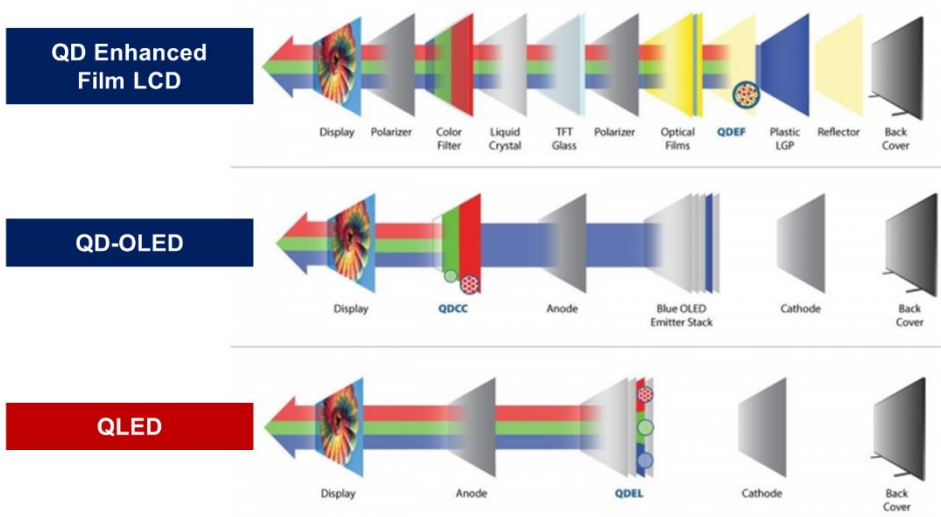

Figure 1.2. Examples of QDs applicable to displays. (Source: Nanosys)

1.3 Structures of Quantum Dot Light-emitting Diodes (QLEDs)

The fabrication methods for QLED devices can be broadly categorized into two types: conventional structure and inverted structure **(Figure 1.3)** [16]. In the conventional structure, the hole injection layer (HIL), hole transport layer (HTL), emitting layer (EML), and electron transport layer (ETL) are sequentially formed on the lower electrode using the spin coating method. Subsequently, the upper electrode is deposited to complete the QLED device. With this method, the lower electrode serves as the anode, while the upper electrode functions as the cathode. The conventional structure offers the advantage of a relatively simple process as the active layers can be fabricated using an all-solution approach. However, in the case of a purely solution-based process, it is crucial to consider solvent orthogonality, as the solvent used for the upper active layer may affect the lower film. Additionally, the conventional structure exhibits a relatively large charge imbalance due to the limited choice of materials available for the solution process.

On the other hand, the inverted structure involves forming the ETL and EML on the lower electrode via the spin coating method. The HTL/HIL is then deposited using the thermal evaporation deposition process within an organic deposition chamber. Finally, the device is completed by depositing the electrode in the metal deposition chamber. In the inverted structure, the lower electrode acts as the cathode, while the upper electrode functions as the anode. Unlike the conventional structure, not all active layers in the inverted structure are formed using a solution process. As a result, it is relatively

unaffected by solvent orthogonality, and it allows for the utilization of various HTL materials that are challenging to deposit via a solution process. Consequently, improving charge balance is comparatively easier. However, the inverted structure does have the drawback of a relatively complex process since some active layers require a solution-based approach, while others necessitate thermal evaporation deposition.

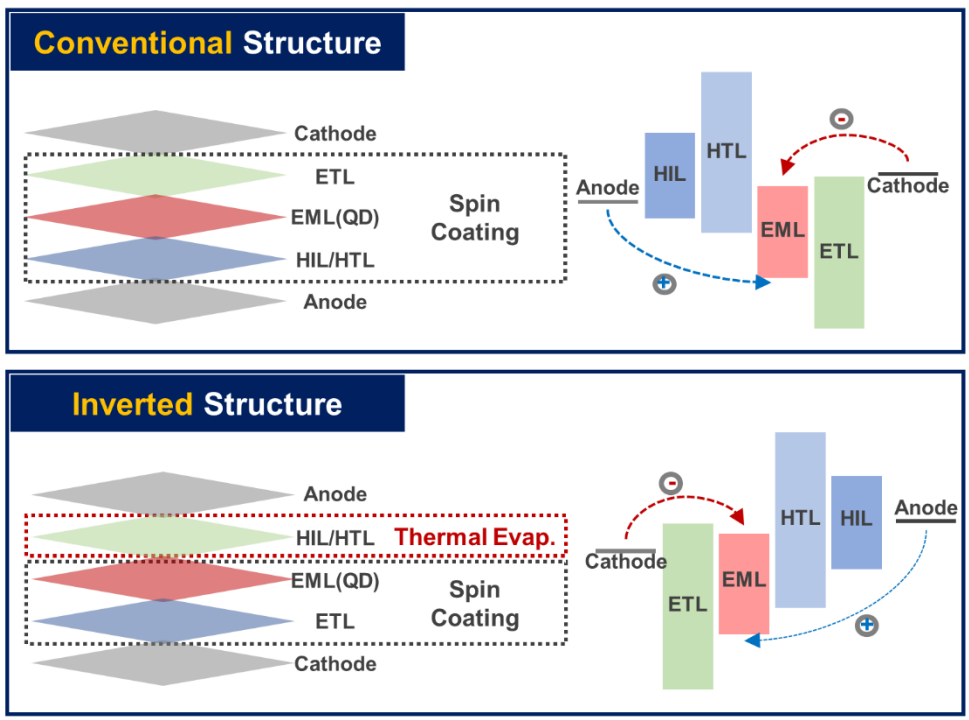

Figure 1.3. Comparison of conventional and inverted structure of QLEDs.

1.4 Main Issues of QLEDs

In the earlier discussion, we mentioned that conventional structure QLEDs exhibit a greater charge imbalance compared to inverted structure QLEDs, and this phenomenon is attributed to the unique energy levels of quantum dots (QDs). Due to their small particle size, QDs are semiconductor materials that possess high reactivity. To ensure stable utilization of QDs and suppress this reactivity, they are designed with a large work function, resulting in deep energy levels. Consequently, the injection barrier encountered by holes injected from the anode is considerably larger than that faced by electrons injected from the cathode. As a result, the QD emitting layer (EML) acquires an electron-rich charge imbalance state, characterized by an excess of electrons relative to holes. This charge imbalance triggers non-radiative recombination, which adversely affects device characteristics. Additionally, it is known that non-radiative recombination can be classified into trap-assisted recombination, interface-induced recombination and Auger recombination. [17-20]. Non-radiative recombination involves the formation of an exciton by an electron and a hole, resulting in the absence of light emission through recombination. Instead, energy is consumed as electrons move to a higher conduction band (electron-electron-hole process) or holes shift to a deeper valence band (hole-hole-electron process) **(Figure 1.4)**. Consequently, recombination does not occur. Auger recombination becomes more pronounced with higher carrier concentrations due to carrier-carrier interactions. Additionally, excess electrons causing HTL degradation are known to have a detrimental impact on device reliability.

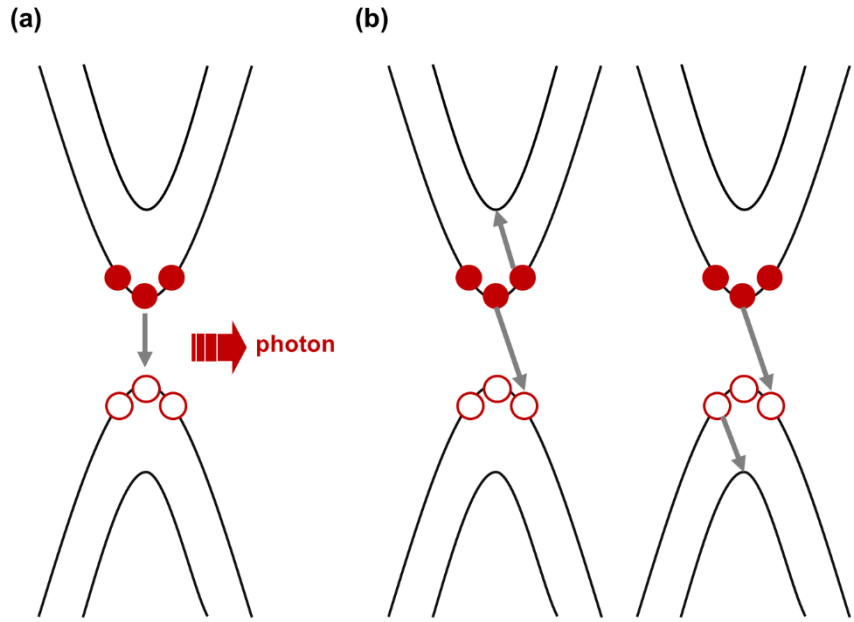

Figure 1.4. Two ways of recombination between excitons in QLEDs. (a) Radiative recombination and (b) non-radiative recombination.

In the case of a conventional structure QLED experiencing a charge imbalance state with an electron predominance, two strategies can be employed to address this imbalance **(Figure 1.5)**. The first strategy involves strong injection of insufficient holes, while the second strategy aims to intentionally suppress the injection of excessive electrons. The first strategy, hole injection enhancement, can be approached in two ways. The first method involves lowering the injection barrier by configuring the energy levels from the hole injection layer (HIL) to the emitting layer (EML) in a cascading manner. The second method entails employing a hole transport layer (HTL) with enhanced hole mobility.

The second strategy, which focuses on suppressing electron injection, can also be achieved through two methods. The first method involves

introducing an interlayer with a high Lowest Unoccupied Molecular Orbital (LUMO) at the interface between the electron transport layer (ETL) and EML, serving as an injection barrier. The second method revolves around utilizing a slower ETL to reduce the electron mobility itself.

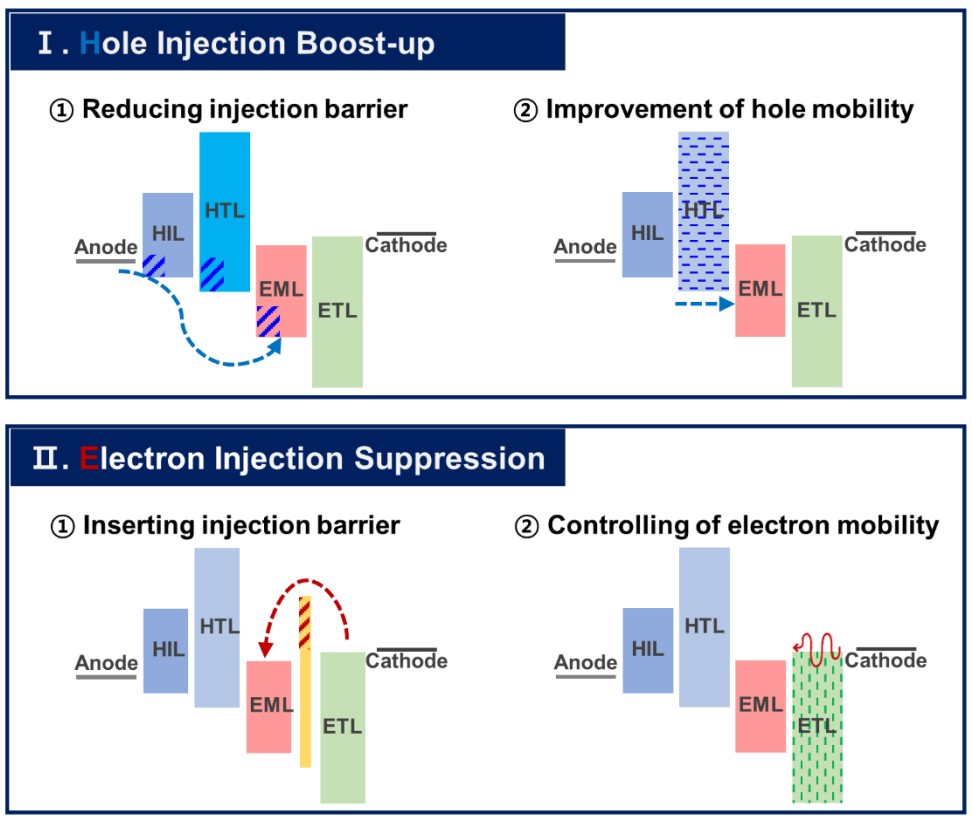

Figure 1.5. Various strategies for improving charge balance.

1.5 Motivation and Organization of This Dissertation

In this study, we propose a method of enhancing the charge balance of conventional structure QLED devices fabricated through a solution process by incorporating various monomers **(Figure 1.6)** through mixing or doping and applying them to the active layer. While the inverted structure exhibits certain advantages in terms of characteristics, the conventional structure holds its own advantages in terms of the fabrication process. Thus, the primary objective of this study was to improve the device characteristics by controlling the charge balance within the conventional structure. Given the diverse range of monomers available, each with unique properties, it was anticipated that the characteristics of the active layer could be precisely controlled by utilizing suitable monomers. Furthermore, adjusting the mixture ratio or doping concentration, rather than altering the materials themselves, offers the advantage of observing gradual changes in the characteristics. However, since the application of monomers typically deposited through thermal evaporation had to be adapted to the solution process, additional factors such as material solubility and glass transition temperature were taken into consideration.

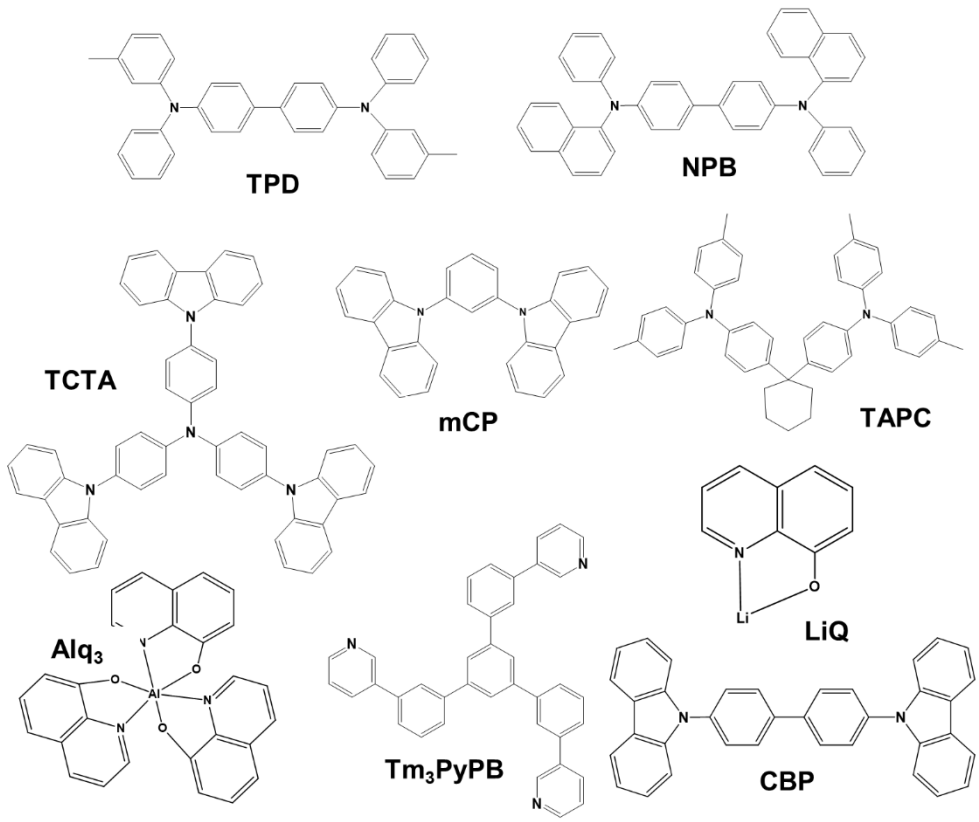

Figure 1.6. Various monomers in OLEDs.

This paper consists of five chapters, including an introduction and a conclusion. Details of each chapter are as follows:

Chapter 1 briefly introduces quantum dots and its applications. In addition, explanations of various displays adopted quantum dots, structure of devices, advantages and disadvantages of each technology, and issues to be overcome were summarized.

Chapter 2 introduces the overall experiment conducted to improve the charge balance of QLEDs fabricated based on solution process. The materials and fabrication methods used in the experiment are described in detail. In addition, the factors used to quantitatively evaluate the fabricated devices and how these factors were extracted are summarized. Various analysis tools used to analyze the characteristics of the devices are also described.

Chapter 3 introduces a method of enhancing the hole injection of QLEDs by mixing a monomer with HTL. This chapter specifically compares and analyzes the effects of the transport and injection abilities of HTL on hole injection into EML.

Chapter 4 presents methods for suppressing electron injection into the EML and ETL interface by inserting an interlayer and doping the ETL with a monomer. We confirmed the effects of each method on the efficiency and operational lifetime of the QLED device, and also provided a detailed description of how the device characteristics change when the two methods are combined.

Chapter 5 finally summarizes the main strategies and achievements of the dissertation. We also mention some limitations, remaining challenges of this study and suggestions for future research.

References

1. C. R. Kagan, E. Lifshitz, E. H. Sargent, and D. V. Talapin, "Building devices from colloidal quantum dots," *Science* **353**, aac5523 (2016).

2. X. Dai, Y. Deng, X. Peng, and Y. Jin, "Quantum-Dot Light-Emitting Diodes for Large-Area Displays: Towards the Dawn of Commercialization," *Adv. Mater.* **29**, 1607022 (2017).

3. Y. E. Panfil, M. Oded, and U. Banin, "Colloidal Quantum Nanostructures: Emerging Materials for Display Applications," *Angew. Chem. Int. Ed.* **57**, 4274–4295 (2018).

4. J. R. Manders, L. Qian, A. Titov, J. Hyvonen, J. Tokarz-Scott, K. P. Acharya, Y. Yang, W. Cao, Y. Zheng, J. Xue, and P. H. Holloway, "High efficiency and ultra-wide color gamut quantum dot LEDs for next generation displays: Quantum dot LEDs for next generation displays," *J. Soc. Info. Disp.* **23**, 523–528 (2015).

5. A. L. Rogach, N. Gaponik, J. M. Lupton, C. Bertoni, D. E. Gallardo, S. Dunn, N. Li Pira, M. Paderi, P. Repetto, S. G. Romanov, C. O'Dwyer, C. M. Sotomayor Torres, and A. Eychmüller, "Light-Emitting Diodes with Semiconductor Nanocrystals," *Angew. Chem. Int. Ed.* **47**, 6538–6549 (2008).

6. Y. Shirasaki, G. J. Supran, M. G. Bawendi, and V. Bulović, "Emergence of colloidal quantum-dot light-emitting technologies," *Nat. Photon.* **7**, 13–23 (2013).

7. T.-H. Kim, C.-S. Lee, S. Kim, J. Hur, S. Lee, K. W. Shin, Y.-Z. Yoon, M. K. Choi, J. Yang, D.-H. Kim, T. Hyeon, S. Park, and S. Hwang, "Fully

Stretchable Optoelectronic Sensors Based on Colloidal Quantum Dots for Sensing Photoplethysmographic Signals," *ACS Nano* **11**, 5992–6003 (2017).

8. J. Kim, H. J. Shim, J. Yang, M. K. Choi, D. C. Kim, J. Kim, T. Hyeon, and D.-H. Kim, "Ultrathin Quantum Dot Display Integrated with Wearable Electronics," *Adv. Mater.* **29**, 1700217 (2017).

9. C.-T. Kung, H. Gao, C.-Y. Lee, Y.-N. Wang, W. Dong, C.-H. Ko, G. Wang, and L.-M. Fu, "Microfluidic synthesis control technology and its application in drug delivery, bioimaging, biosensing, environmental analysis and cell analysis," *J. Chem. Eng.* **399**, 125748 (2020).

10. K. Hagiwara, S. Horikoshi, and N. Serpone, "Luminescent monodispersed carbon quantum dots by a microwave solvothermal method toward bioimaging applications," *J. Photochem. Photobio. A: Chem.* **415**, 113310 (2021).

11. A. R. Kirmani, J. M. Luther, M. Abolhasani, and A. Amassian, "Colloidal Quantum Dot Photovoltaics: Current Progress and Path to Gigawatt Scale Enabled by Smart Manufacturing," *ACS Energy Lett.* **5**, 3069–3100 (2020).

12. M. Liu, M. Liu, X. Wang, S. M. Kozlov, Z. Cao, P. De Luna, H. Li, X. Qiu, K. Liu, J. Hu, C. Jia, P. Wang, H. Zhou, J. He, M. Zhong, X. Lan, Y. Zhou, Z. Wang, J. Li, A. Seifitokaldani, C. T. Dinh, H. Liang, C. Zou, D. Zhang, Y. Yang, T.-S. Chan, Y. Han, L. Cavallo, T.-K. Sham, B.-J. Hwang, and E. H. Sargent, "Quantum-Dot-Derived Catalysts for CO_2 Reduction Reaction," *Joule* **3**, 1703–1718 (2019).

13. J. Lim, Y.-S. Park, and V. I. Klimov, "Optical gain in colloidal quantum dots achieved with direct-current electrical pumping," *Nature Mater.* **17**, 42–49 (2018).

14. X. Tang, M. M. Ackerman, M. Chen, and P. Guyot-Sionnest, "Dual-band infrared imaging using stacked colloidal quantum dot photodiodes," *Nat. Photon.* **13**, 277–282 (2019).

15. J. Yang, M. K. Choi, U. J. Yang, S. Y. Kim, Y. S. Kim, J. H. Kim, D.-H. Kim, and T. Hyeon, "Toward Full-Color Electroluminescent Quantum Dot Displays," *Nano Lett.* **21**, 26–33 (2021).

16. G. W. Baek, Y. J. Kim, M. Lee, Y. Kwon, B. Chun, G. Park, H. Seo, H. Yang, and J. Kwak, "Progress in the Development of Active-Matrix Quantum-Dot Light-Emitting Diodes Driven by Non-Si Thin-Film Transistors," *Materials* **15**, 8511 (2022).

17. B. S. Mashford, M. Stevenson, Z. Popovic, C. Hamilton, Z. Zhou, C. Breen, J. Steckel, V. Bulovic, M. Bawendi, S. Coe-Sullivan, and P. T. Kazlas, "High-efficiency quantum-dot light-emitting devices with enhanced charge injection," *Nature Photon* **7**, 407−412 (2013).

18. W. K. Bae, Y.-S. Park, J. Lim, D. Lee, L. A. Padilha, H. McDaniel, I. Robel, C. Lee, J. M. Pietryga, and V. I. Klimov, "Controlling the influence of Auger recombination on the performance of quantum-dot light-emitting diodes," *Nat. Commun.* **4**, 2661 (2013).

19. W.-C. Chao, T.-H. Chiang, Y.-C. Liu, Z.-X. Huang, C.-C. Liao, C.-H. Chu, C.-H. Wang, H.-W. Tseng, W.-Y. Hung, and P.-T. Chou, "High efficiency green InP quantum dot light-emitting diodes by balancing electron and hole mobility," *Commun. Mater.* **2**, 96 (2021).

20. H. Cheng, Y. Feng, Y. Fu, Y. Zheng, Y. Shao, and Y. Bai, "Understanding and minimizing non-radiative recombination losses in perovskite light-emitting diodes," *J. Mater. Chem. C* **10**, 13590–13610 (2022).

Chapter 2

Experimental Section

2.1 Materials

The materials used in the fabrication of the QLED device are as follows. Isopropyl alcohol (IPA, Daejung Chemicals & Metals Co.) and acetone (Daejung Chemicals & Metals Co.) were used for substrate cleaning without additional purification. We used Poly(3,4-ethylenedioxythiophene):poly(styrenesulfonate) (PEDOT:PSS, AI4083, Heraeus) as the HIL to form the functional layers of QLED. Poly(N-vinylcarbazole) (PVK, Sigma Aldrich Co.), 4,4',4"-tris(N-carbazolyl)-triphenylamine (TCTA, Tokyo Chemical Industry Co.) and 1,3-Di-9-carbazolylvenzene (mCP, Tokyo Chemical Industry Co.) were used as HTL. We used red quantum dots (quantum yield ~90 %, ZEUS) with an oleic acid ligand and CdSe/ZnS core-shell structure to form the EML. The absorption and photoluminescence (PL) emission spectra are illustrated in **Fig. 2.1(a)**. A CdSe/ZnS QD has a wide absorption spectrum in the visible region. The peak wavelength of PL is located at 620 nm, and the full width at half maximum has a highly narrow spectrum at approximately 32 nm. As shown in the TEM image in **Fig. 2.1(b)**, the average size of the CdSe/ZnS QDs was determined to be 8 nm, and it was confirmed that they were spherically shaped with a uniform size distribution. Polyethylenimine (PEI, Sigma Aldrich) was used

as an interlayer. Zinc oxide nanoparticles dispersed in buthanol (ZnO NP, N-13, Avantama) and (8-Quinolinolato)lithium (LiQ, Tokyo Chemical Industry Co.) were used as ETL for the QLED device. The phase and morphology of the nanoparticles of ZnO used in this experiment were analyzed by using an X-ray diffractometer and CS-TEM. The related data are presented in **Fig. 2.2**. After spin-coating, the subsequent process involved depositing the cathode using thermal evaporation in a vacuum chamber. For this purpose, LiF (Itasco) as EIL and Al (Itasco) as cathode were used.

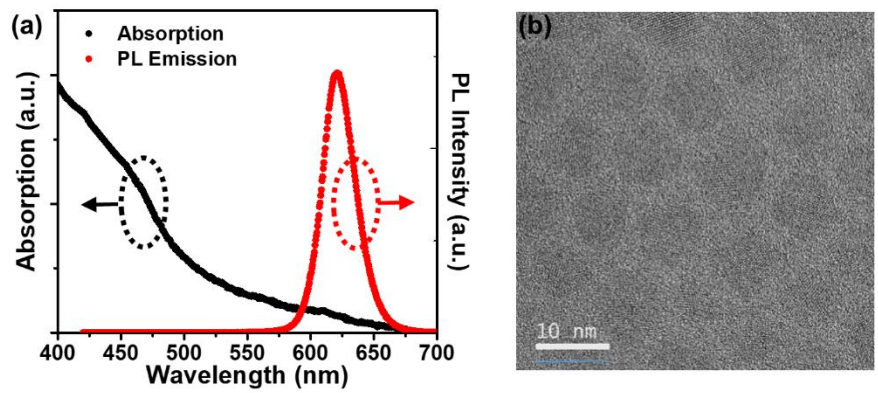

Figure 2.1. (a) Absorption and PL spectra and (b) TEM image of the QDs.

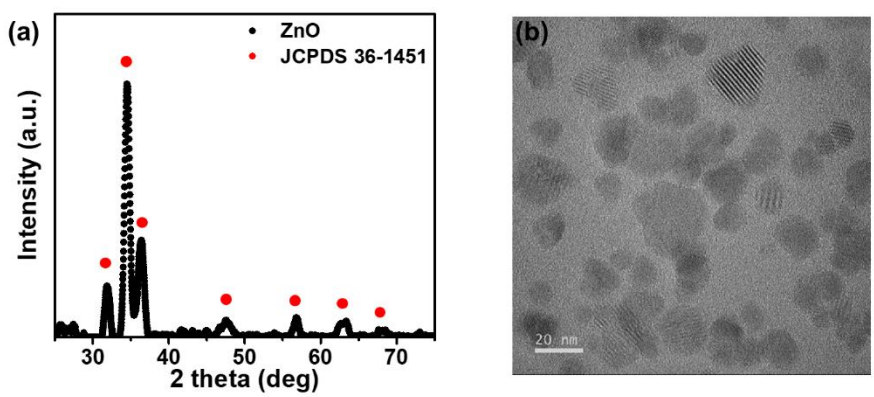

Figure 2.2. (a) XRD pattern and (b) TEM image of the ZnO nanoparticles.

2.2 Fabrication of QLEDs

The structure of the QLED reference device used in the experiment is shown in **Fig. 2.3**.

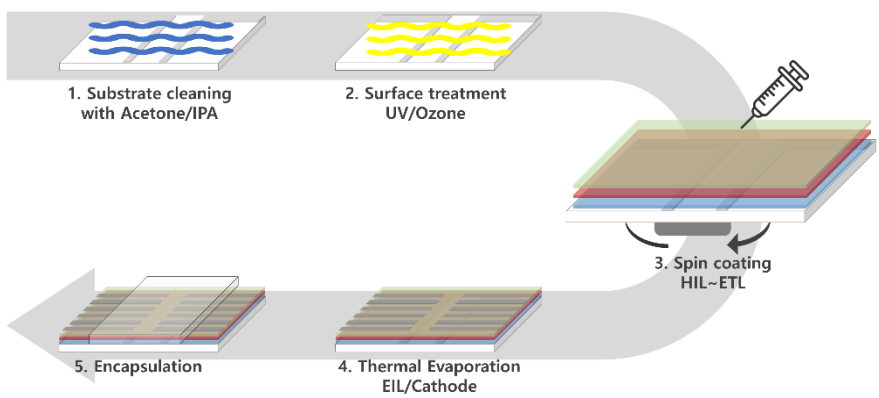

Figure 2.3. Fabrication schematic of QLEDs.

An indium tin oxide (ITO)-patterned glass substrate was used to fabricate the device. The substrate was sequentially cleaned using a sonicator with acetone/isopropyl alcohol/deionized water for 15 min before fabrication and then dried for approximately 1 h in an oven at 100 °C. Subsequently, thermal treatment was performed for 1 h in an air atmosphere inside a furnace at 350 °C. Upon applying ultraviolet/ozone surface treatment for 5 min to obtain a uniform deposition, the substrate was placed in a glove box in an Ar atmosphere to fabricate the device with the structure shown in **Fig. 2.4(a)**. PEDOT:PSS was used as a HIL by spin coating at 2000 rpm for 60 s before annealing at 120 °C for 30 min. PVK (2 mg/ml in chloroform) was used as an HTL by coating at 4000 rpm for 30 s and annealing at 100 °C for 30 min. To deposit the HTL mixed with a monomer, TCTA or mCP were dissolved in

chloroform at a concentration of 2 mg/mL, and a solution mixed with 2 mg/mL of PVK in volume ratio was used. The EML of the QD (20 mg/ml in octane) was coated at 2000 rpm for 60 s and then annealed at 80 °C for 30 min. PEI (0.1 mg/ml in IPA) was used as an interlayer by coating at 5000 rpm for 50 s and then annealing at 100 °C for 30 min. ZnO (40 mg/ml in Butanol) was coated as an ETL at 4000 rpm for 30 s and then annealed at 100 °C for 30 min. Once spin coating was complete, the device was transferred to a vacuum chamber to form a cathode with LiF (1 nm)/Al (80 nm) in a 10^{-7} Torr atmosphere. The fabricated QLED devices were then encapsulated using ultraviolet-curable resin and cavity glass to prevent degradation owing to moisture and oxygen. Finally, the device characteristics were evaluated.

The structure of the QLED device fabricated through the above process is shown in **Fig. 2.4(a)**, which serves as a reference structure for the studies discussed in chapter 3 and 4. The thickness and composition of each layer in the solution-processed QLEDs were confirmed by observing cross-section views using TEM and analyzing the elemental composition using EDS as shown in **Fig. 2.4(b)** and **Fig. 2.5**.

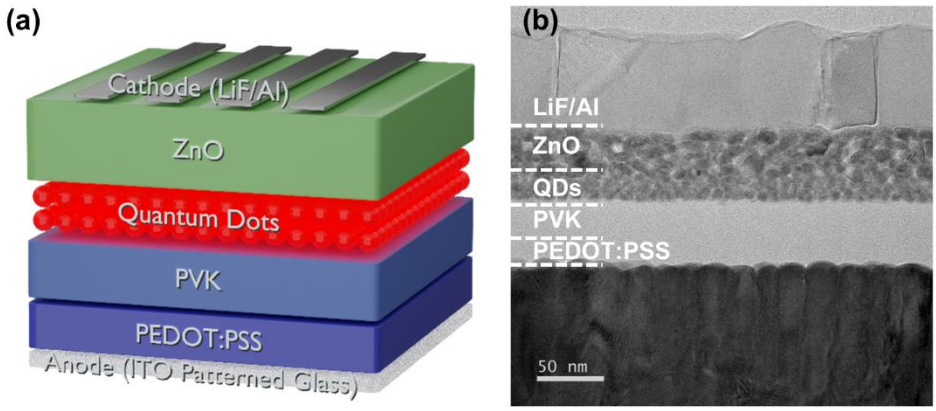

Figure 2.4. (a) Device structure of multi-layered QLEDs and (b) cross-sectional TEM image of the device.

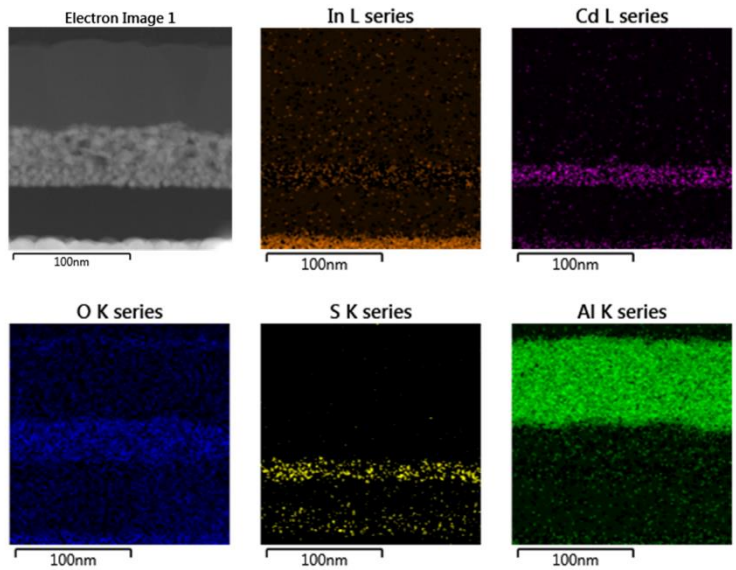

Figure 2.5. Cross-sectional EDS image of the device.

2.3 Characterization of QLEDs

2.3.1 Current density-Voltage-Luminance (*J-V-L*) Measurement

The electrical characteristics (Current-Voltage (*J-V*)) of the device were measured via the voltage sweeping method using the source measurement unit (Keithley 236, Keithley). The electroluminescence was measured by placing the Si photodiode (Hamamatsu, S5227-1010BQ) connected to a digital multimeter (Keithley 2000, Keithley) perpendicular to the device to extract the photocurrent according to the applied voltage. Then, the luminance, efficiency, and color coordinates were calculated based on the photocurrent obtained through the photodiode and luminance measured by the spectroradiometer (CS-2000, Konica Minolta).

There are various criteria for evaluating the luminous characteristics of fabricated devices. However, in this paper, we mainly used current efficiency, power efficiency, and external quantum efficiency calculated based on the *J-V-L* characteristics of the fabricated devices. The human eye has a different sensitivity depending on the wavelength of the visible light range, and the International Commission on Illumination (CIE) standardized this sensitivity and named it as 'luminous efficiency function **(Figure 2.6)**'. The current efficiency and power efficiency reflect this luminous efficiency function, and the equations for calculating them are as follows.

$$\text{Current Efficiency} = \frac{luminance}{current\ \ density} \quad (cd/A)$$

$$\text{Power Efficiency} = \frac{luminous\ \ flux}{power}\ \ (lm/W)$$

If the current efficiency is a suitable method for evaluating the basic characteristics of a light-emitting device, the power efficiency is a more practical method that can be applied to and used in mass production because it includes power consumption. In addition, external quantum efficiency (EQE) is widely employed as a factor for evaluating the characteristics of light-emitting diodes. The EQE of a light-emitting diode represents the ratio of photons emitted from a luminescent device to the injected electrons within the device, and it is expressed by the following equation.

$$\text{External Quantum Efficiency} = \frac{\#\ of\ \ photons\ \ out}{\#\ of\ \ electrons\ \ in} = \frac{P/h\nu}{I/e}\ \ (\%)$$

In the above equation, P refers to the total power of photons, h is planck constant, ν is the frequency of photon, I is injected current and e represents the elementary charge. If the current efficiency and power efficiency are methods that reflect many environmental factors such as luminosity factor and light extraction efficiency, the external quantum efficiency is a factor that best represents the intrinsic characteristics of the device.

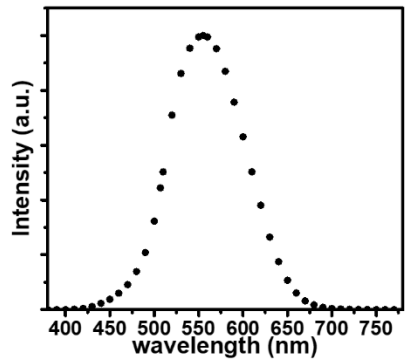

Figure 2.6. Luminous efficiency function.

The color coordinates of light-emitting devices, as well as their luminous efficiency, must be considered in depth for applications in the display industry. This is because color coordinates greatly affect the brightness and color perceived by the human eye. There are several methods for defining color coordinates based on research on the human perception of color. However, the CIE 1931 color coordinates established by the CIE in 1931 is the most widely used method. To define color coordinates, we first need tristimulus values (*X, Y,* and *Z*), which can be expressed as the following equation.

$$X = \mathrm{K}\int_0^\infty I(\lambda)\bar{x}(\lambda)d(\lambda)$$

$$Y = \mathrm{K}\int_0^\infty I(\lambda)\bar{y}(\lambda)d(\lambda)$$

$$Z = \mathrm{K}\int_0^\infty I(\lambda)\bar{z}(\lambda)d(\lambda)$$

$I(\lambda)$: The emission spectrum of light-emitting diodes

$\bar{x}$, $\bar{y}$, $\bar{z}(\lambda)$: CIE standard color matching functions **(Figure 2.7)**.

The CIE color coordinates (x, y, and z) can be calculated with the above tristimulus values as follows.

$$x = \frac{X}{X + Y + Z}$$

$$y = \frac{Y}{X + Y + Z}$$

$$z = \frac{Z}{X + Y + Z} = 1 - (x + y)$$

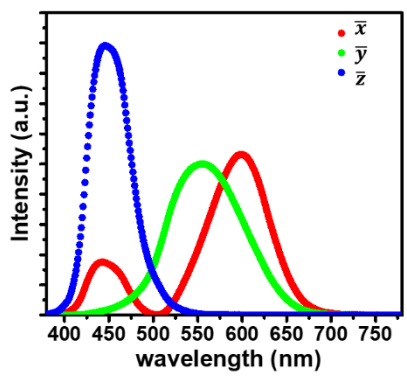

Figure 2.7. CIE standard color matching function.

Figure 2.8 shows the chromaticity distribution diagram of the CIE 1931 color space plotted with x and y as variables. The outer boundary represents monochromatic light, and the wavelength of each monochromatic light is expressed in nm.

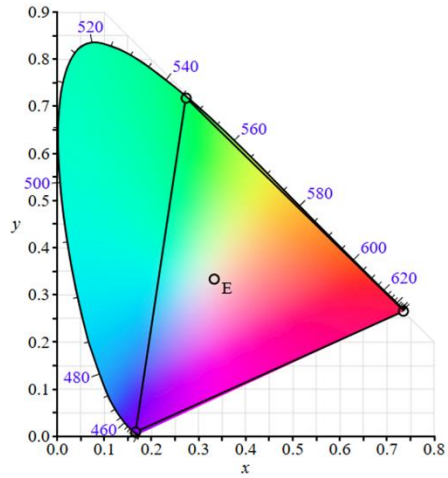

Figure 2.8. CIE 1931 color space.

2.3.2 Operational Lifetime

In order to check how stable the characteristics of the fabricated light-emitting device are according to the driving time, the room-temperature operational lifetime of the device was evaluated. The evaluation was conducted using M3600 by McScience, which consists of a thermo-hygrostat chamber and a jig to which a photodiode was attached as shown in **Fig. 2.9**. After mounting the device on the jig, a constant current was applied to extract the light emitted by the device in the form of a photocurrent. Then we observed how the luminous characteristics of the device changed over time.

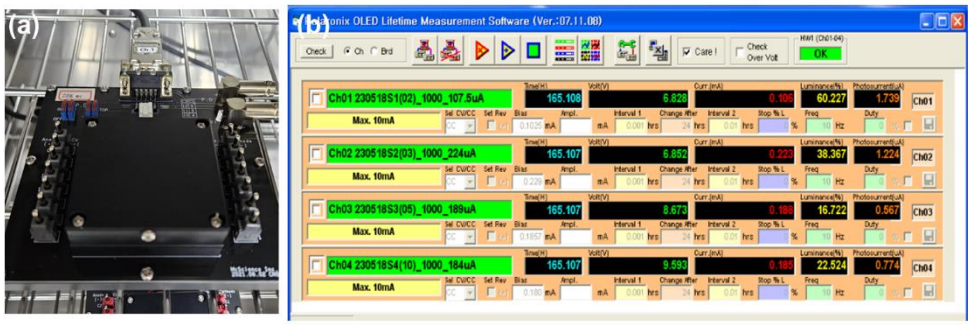

Figure 2.9. (a) The camera image of M3600 and (b) its operating program.

2.3.3 Other Characterization Methods

We used transmission electron microscopy (Cs-TEM, JEM-ARM200F, JEOL Ltd) to verify the cross-section of the fabricated devices and morphologies of the nanoparticles. Furthermore, the absorption and emission spectra were obtained using ultraviolet–visible spectroscopy (Lambda35, Perkin Elmer) and photoluminescence equipment (Photoluminescence, FlouTime300, PicoQuant) to determine the optical properties of the QD emitter. The surface roughness was observed using an atomic force microscope (XE-150, PSIA), and ultraviolet photoelectron spectroscopy (AXIS SUPRA, Kratos, U.K.) measurements were acquired for energy level analysis. An X-ray diffractometer (D8 Advance, Bruker) was utilized to conduct a phase analysis of the inorganic material.

Chapter 3

Monomer-mixed Hole Transport Layers for Improving Hole Injection of Quantum Dot Light-emitting Diodes

3.1 Introduction

Strengthening hole injection has been extensively studied **(Figure 3.1)**, with the most widely known method being the application of an inverted structure [1]. It entails coating the ETL/EML using a solution process and subsequently depositing the monomer for organic LEDs onto the EML via thermal evaporation to complete the device. Furthermore, studies have been conducted to enhance the injection properties by cross-linking HTL materials [2-10] or by creating a multilayer structure that involves the hole injection layer (HIL) and HTL to control the hole injection barrier [11-17]. Alternatively, hole injection has been enhanced by controlling the HTL properties using various additives such as Lewis acid [18], Lithium-TFSI [19], 1,1-Bis[(di-4-tolylamino)phenyl]cyclohexane (TAPC) [20-22], 4,4'-Bis(N-carbazolyl)-1,1'-biphenyl (CBP) [23-25], and poly[bis(4-phenyl)(2,4,6-trimethylphenyl)amine] (PTAA) [26] within the HTL. In particular, the wherein additives were mixed and applied to the HTL have shown that the hole injection into the EML is strengthened and that the device characteristics

are improved. However, it is difficult to accurately analyze and determine whether the improvement in device characteristics is because of the change in the hole mobility of the HTL or because of the change in the injection barrier from HTL to EML.

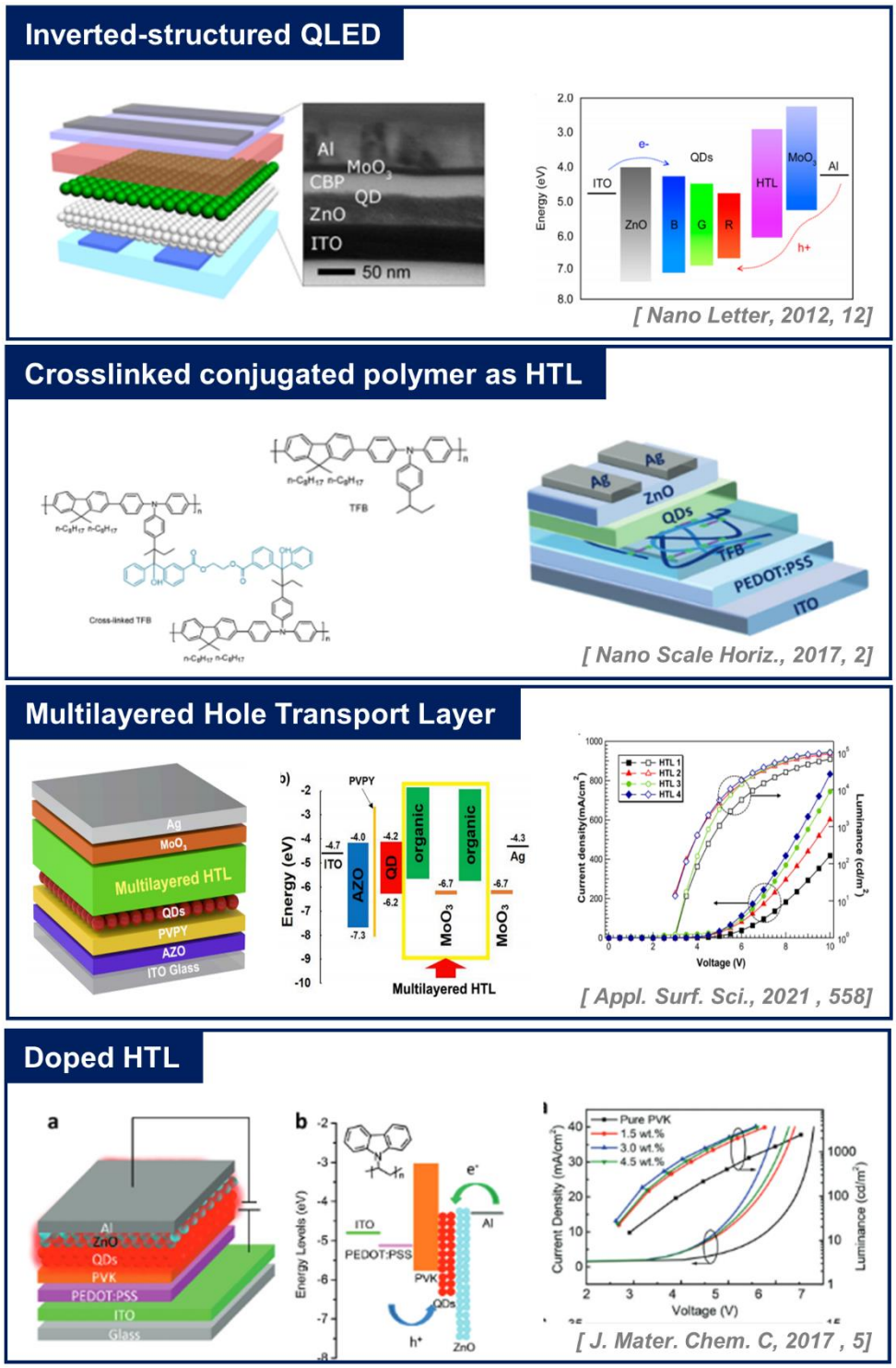

Figure 3.1. Various studies on enhancing hole injection in QLEDs [1, 7, 12, 19].

In this study, we combined two different monomers, namely, 4,4',4"-tris(N-carbazolyl)-triphenylamine (TCTA) and 1,3-Di-9-carbazolylvenzene (mCP), with poly(N-vinylcarbazole) (PVK) to enhance the device characteristics by strengthening the hole injection. Subsequently, the combinations were applied to the HTL, and the devices were evaluated. To enhance the hole injection into the EML, we considered both the application of the HTL with high hole mobility and the reduction of the injection barrier owing to the formation of a gradual energy level. As the monomer was deposited via a solution process rather than thermal deposition, the impacts of the material on the process, such as solubility or glass transition temperature, were considered. Moreover, the effects of related phenomena on the device properties were also analyzed. When TCTA and mCP were mixed with PVK and applied as HTLs, the charge balance of the device improved with the strengthened hole injection. Consequently, the current and power efficiency was improved by 24% and 52%, respectively.

The structure of the QLED used in the experiment and a transmission electron microscopy image are shown in **Fig. 2.4(a)**. QLEDs fabricated by the all-solution process had the structure of ITO/PEDOT:PSS (20 nm)/PVK or PVK:monomer (25 nm)/QDs (20 nm)/ZnO (35 nm)/LiF (1 nm)/Al (80 nm). The hole was injected through the ITO anode, and the electron was inserted into the device through the Al cathode. PEDOT:PSS was used as the HIL, PVK or PVK:monomer as the HTL, QD as the EML, and ZnO as the ETL. The molecular structures of TCTA and mCP mixed with PVK, which constitute the HTL to enhance hole injection, are shown in **Fig. 3.2(a)**, and the flat-band energy level diagram including TCTA and mCP is shown in **Fig. 3.2(b)**. The detailed properties of the materials are summarized in **Table. 3.1**

[27-30]. The highest occupied molecular orbital (HOMO) and lowest unoccupied molecular orbital (LUMO) reported in other studies were used to characterize materials [20, 21]. The hole mobility of PVK used as HTL was 2.5×10^{-6} $cm^2/V{\cdot}s$, which is much slower than that of ZnO (10^{-3} – 10^{-4} $cm^2/V{\cdot}s$) and disadvantageous for both injection and transport. As TCTA has a shallower HOMO than PVK, it cannot reduce the injection barrier from the HTL to the EML. However, because TCTA has a higher hole mobility of 4×10^{-4} $cm^2/V{\cdot}s$ than that of PVK, it was expected to deliver a hole quickly to the EML. Moreover, mCP, whose HOMO is deeper than that of PVK, can reduce the injection barrier from the HTL to the EML. Hence, mCP was expected to contribute to the improvement of both injection and transport because it has a higher mobility (3.4×10^{-5} $cm^2/V{\cdot}s$) than that of PVK.

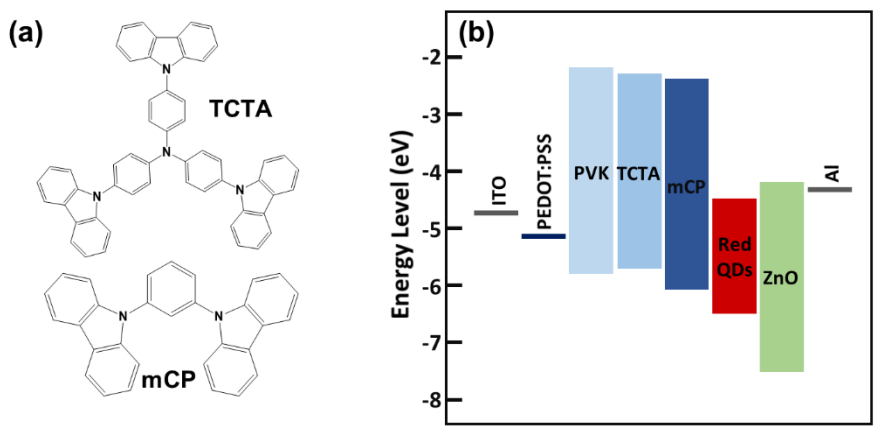

Figure 3.2. (a) Molecular structures of TCTA and mCP. (b) Energy level diagram for various layers of the QLEDs.

Device	PVK	TCTA	mCP
HOMO (eV)	-5.8	-5.7	-6.1
LUMO (eV)	-2.2	-2.3	-2.4
T_g (℃)	-	155	64
Hole mobility ($cm^2/V·s$)	2.5×10^{-6}	4.0×10^{-4}	3.4×10^{-5}

Table 3.1. Physical properties of used materials [27-30].

3.2 Results and Discussion

3.2.1 TCTA mixed HTL

To investigate the effect of HTL mixed with TCTA on the device properties, devices were fabricated by mixing TCTA with PVK in concentrations of 10%–40%. **Figure 3.3** shows the performance of the fabricated devices. **Figure 3.3(a)** shows that as the mixing ratio of the TCTA increased, the current density in the applied voltage tended to increase along with the luminance. To further clarify the luminescence characteristics in the low-voltage region, the luminance versus voltage in the light turn-on region (~100 cd/m^2) is plotted on the inset graph of **Fig. 3.3(a)**. It can be confirmed that as the concentration of the TCTA increased, a shift occurred in the direction of a decrease in light turn-on voltage. An increase in current density and decrease in turn-on voltage indicated that hole injection enhanced with the TCTA mixture. The highest improvement in efficiency was obtained for the device mixed with 20% TCTA. The current efficiency for the mixture was 6.56 cd/A, being 24% higher than that of the PVK-only device (5.29 cd/A). The external quantum efficiency was found to be 4.99 %, which represents a 23 % improvement compared to the reference, 4.04 %. Moreover, when TCTA was mixed, the current, power, and external quantum efficiencies increased. For the 30% TCTA mixture, the current efficiency decreased compared with the 20% TCTA mixture. As hole injection further improved, the effect of reducing the driving voltage increased the power efficiency by

52% compared with the PVK-only device. The detailed properties of the device per condition are summarized in **Table 3.2**.

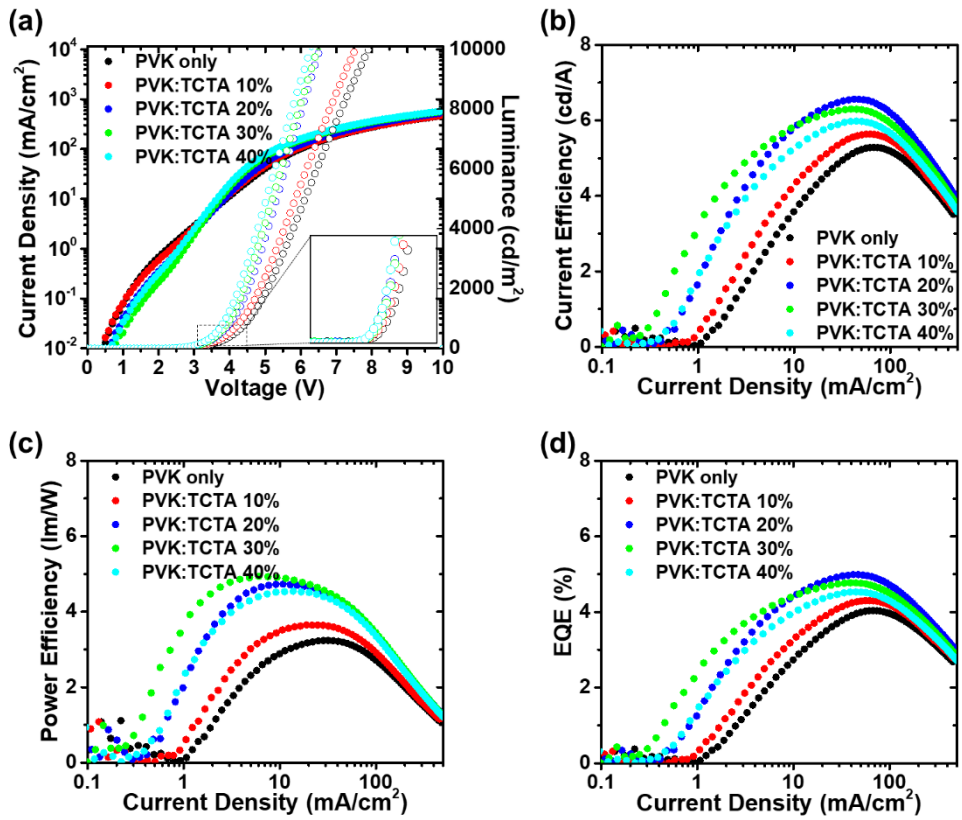

Figure 3.3. Electroluminescence (EL) performance of the QLEDs with PVK or PVK:TCTA HTLs. (a) Current density-voltage-luminance (*J-V-L*) characteristics, inset shows voltage-luminance (*V-L*) in the range under 100 cd/m^2. (b) Current efficiency-current density characteristics. (c) Power efficiency-current density characteristics. (d) External quantum efficiency-current density characteristics.

Device	V_{on} (V)	V_d (V)	Max CE (cd/A)	Max PE (lm/W)	Max EQE (%)	λ_{max} (nm)	CIE coordinate (x,y)
PVK only	2.3	4.5	5.29	3.24	4.04	626	(0.68, 0.32)
PVK:TCTA 10 %	2.2	4.3	5.64	3.65	4.30	626	(0.68, 0.32)
PVK:TCTA 20 %	2.1	4.1	6.56	4.73	4.99	626	(0.68, 0.32)
PVK:TCTA 30 %	2.1	4.0	6.30	4.93	4.77	626	(0.68, 0.32)
PVK:TCTA 40 %	2.1	3.8	5.98	4.54	4.53	626	(0.68, 0.32)

[a] V_{on} is the turn-on voltage corresponding to 1 cd/m^2, and V_d is the driving voltage corresponding to 1000 cd/m^2.

Table 3.2. Performance summary of QLEDs with various HTLs.

Figure 3.4(a) shows the electroluminescence spectra of the device by mixing ratio. And **Fig. 3.4(b)** shows the electroluminescence spectrum of the PVK:TCTA 20% device by voltage. The peak wavelength of electroluminescence was located at 626 nm, and no changes in the spectrum occurred even when the mixing ratio and driving voltage were changed. Moreover, the absence of other emission peaks indicates that excitons were suitably confined inside the QD EML and smoothly recombined. When compared with the PL spectrum in **Fig. 2.1(a)**, the central wavelength redshifted by approximately 6 nm due to the quantum confined Stark effect in the QD layer [31].

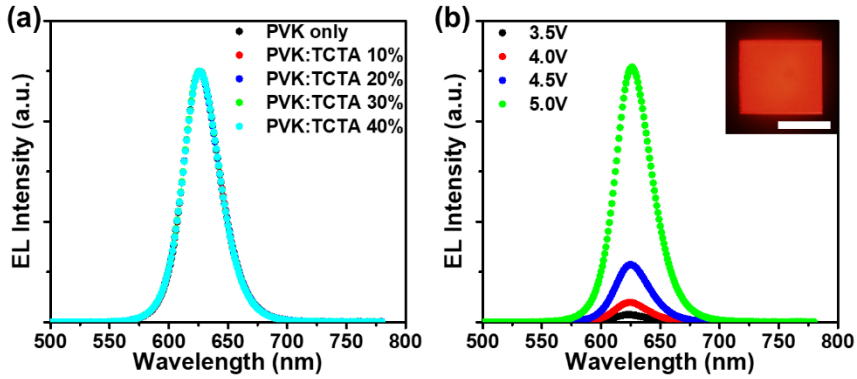

Figure 3.4. EL spectra of (a) QLED with various concentration of TCTA and (b) QLED with a PVK:TCTA 20%, as a function of the applied voltage. The inset shows a light-emitting image of the device, with a scale bar of 1mm.

3.2.2 mCP mixed HTL

The electroluminescence of the device with PVK:mCP HTL is shown in **Fig. 3.5**. Similar to the experiment conducted with the TCTA mixture, by increasing the mixing ratio of mCP, the current density and luminance increased at an applied voltage. The PVK:mCP device exhibits the highest performance for the 30% mCP mixture. Compared with the PVK-only device, the current efficiency improved by 20% (from 5.38 cd/A to 6.49 cd/A), and the power efficiency improved by 47% (from 3.01 lm/W to 4.43 lm/W) and the external quantum efficiency was improved by 20 % (from 4.13 % to 4.96 %). The detailed properties of the device per condition are summarized in **Table 3.3**.

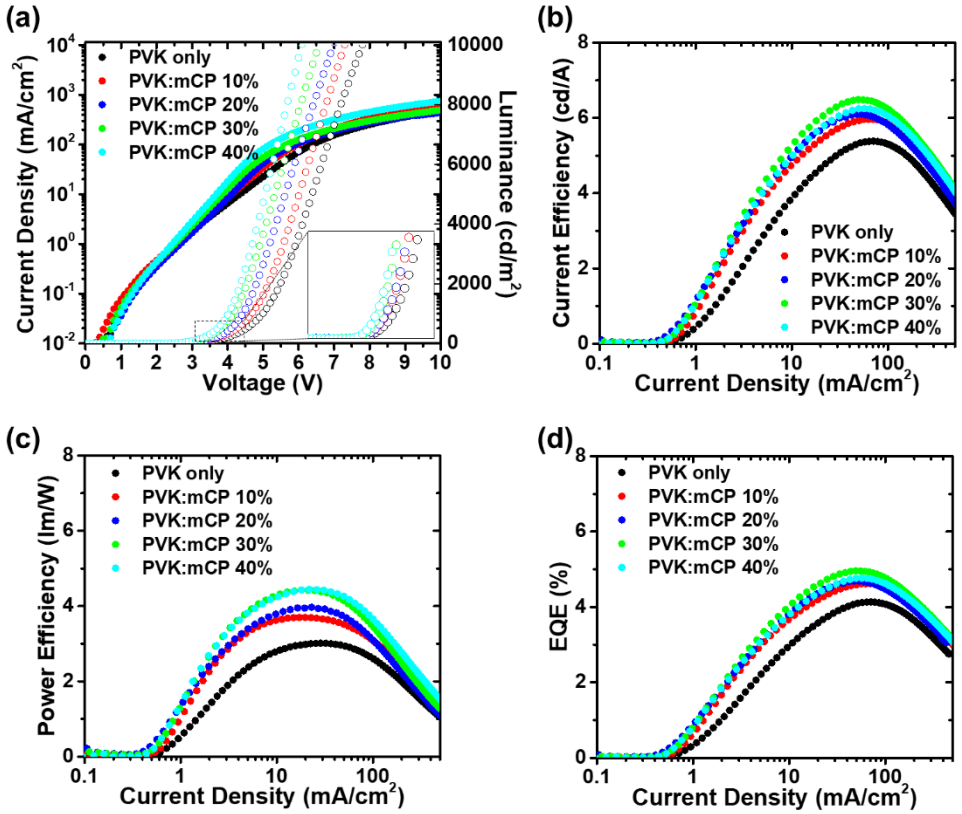

Figure 3.5. Electroluminescence (EL) performance of the QLEDs with PVK or PVK:mCP HTLs. (a) Current density-voltage-luminance (*J-V-L*) characteristics, inset shows voltage-luminance (*V-L*) in the range under 100 cd/m^2. (b) Current efficiency-current density characteristics. (c) Power efficiency-current density characteristics. (d) External quantum efficiency-current density characteristics.

Device	V_{on} (V)	V_d (V)	Max CE (cd/A)	Max PE (lm/W)	Max EQE (%)	λ_{max} (nm)	CIE coordinate (x,y)
PVK only	2.3	4.7	5.38	3.01	4.13	626	(0.68, 0.32)
PVK:mCP 10 %	2.2	4.4	5.97	3.70	4.62	626	(0.68, 0.32)
PVK:mCP 20 %	2.2	4.2	6.10	3.97	4.69	626	(0.68, 0.32)
PVK:mCP 30 %	2.1	3.9	6.49	4.43	4.96	626	(0.68, 0.32)
PVK:mCP 40 %	2.1	3.8	6.25	4.44	4.77	626	(0.68, 0.32)

[a] V_{on} is the turn-on voltage corresponding to 1 cd/m^2, and V_d is the driving voltage corresponding to 1000 cd/m^2.

Table 3.3. Performance summary of QLEDs with various HTLs.

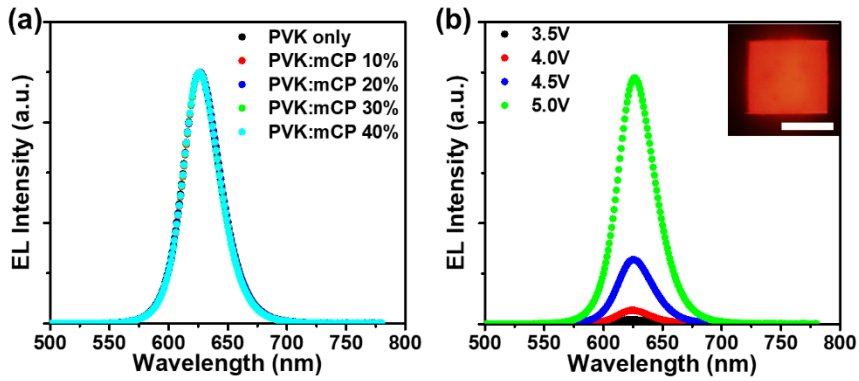

Figure 3.6. EL spectra of (a) QLED with various concentration of mCP and (b) QLED with a PVK:mCP 20%, as a function of the applied voltage. The inset shows a light-emitting image of the device, with a scale bar of 1mm.

3.2.3 Comparative Analysis of Properties

The surface roughness was measured with an atomic force microscope to check for changes in the film quality when each of the two monomers was applied to the HTL. The contact interface properties between two layers are critical for determining the properties of a multilayer film device. Suitable interface properties are essential for QLEDs fabricated via spin coating [13, 32]. **Figure 3.7** shows the measurement results of surface roughness in the HTL. When roughness root mean square (R_q) of the reference layer (with PVK only) was 0.901 nm, the surface roughness of the PVK:TCTA HTL was 0.668 nm, and the surface roughness of the PVK:mCP layer was 1.268 nm. All of these values indicate that a sufficiently flat surface was obtained when different HTLs were coated via the spin coating process. Nevertheless, the difference in the roughness of thin films may be attributed to the glass transition temperature (T_g) of each monomer [30]. For the TCTA, T_g is extremely high at 155 °C, and the surface is smoothened even if it is mixed with PVK and spin coated before annealing at 100 °C. On the other hand, mCP appears to increase the surface roughness as crystallization occurs in part of the annealing process because T_g is very low at 64 °C.

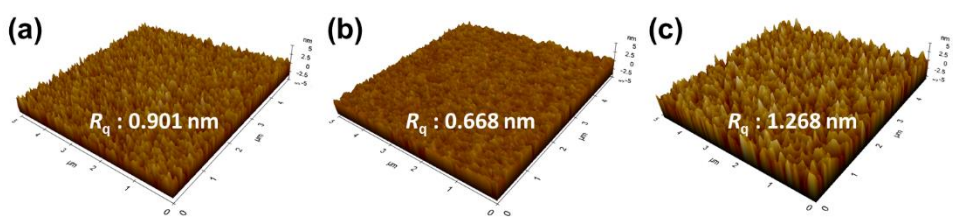

Figure 3.7. AFM images and surface roughness values of different HTLs (a) PVK only. (b) PVK:TCTA 20%. (c) PVK:mCP 20%.

A hole-only device was fabricated to observe the behavior of the hole injected into the EML and identify the underlying reason for the improvement in the device properties by doping a monomer into the PVK HTL. The hole-only device had the structure of ITO/PEDOT:PSS (20 nm)/HTLs (25 nm)/EML (20 nm)/MoO_3 (1 nm)/Al (50nm). The structure was used to compare different properties, including hole transport in the HTL and injection in the EML. **Figure 3.8(a)** and **Figure 3.8(b)** show the hole-only devices of PVK:TCTA and PVK:mCP according to the mixing concentration. An increased current density with the TCTA or mCP concentration in the mixture with PVK can be clearly identified in both devices. Hence, hole injection in the EML was strengthened. This is also consistent with the current density–voltage (*J-V*) properties of the QLED device, as shown in **Fig. 3.3(a)** and **Fig. 3.5(a)**.

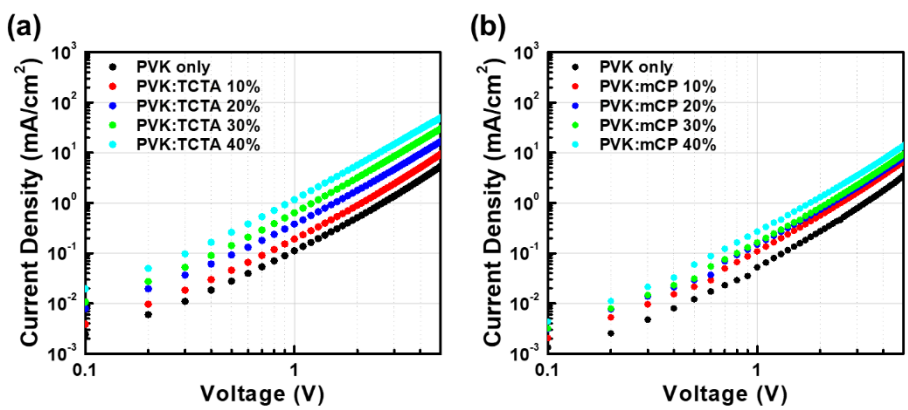

Figure 3.8. Current density-Voltage (*J-V*) characteristics of the hole only devices (HODs) with different HTLs for (a) PVK:TCTA and (b) PVK:mCP.

In addition, to quantitatively compare the hole transport ability owing to the monomer mixture, we extracted mobility from the *J-V* curve of the HODs. The following equation was utilized to extract mobility (μ).

$$J = \frac{9}{8}\varepsilon_0\varepsilon_r\mu\frac{V^2}{d^3}$$

In the above equation, *J* refers to the current density in space charge limited current (SCLC) region, and *V* represents the applied voltage. ε_0 and ε_r denote the vacuum dielectric constant (8.85×10^{-14} C/V·cm) and the relative dielectric constant, respectively. In this study, an ε_r value of 3 was applied for the organic material [13, 26]. Additionally, *d* represents the distance between the anode and cathode. Based on the *J-V* curve of the hole-only device, the calculated mobility values were 8.32×10^{-7} cm^2/V·s for the PVK only device, 1.44×10^{-6} cm^2/V·s for the PVK:TCTA 20 % device, and 1.12×10^{-6} cm^2/V·s for the PVK:mCP 20 % device. It was observed that the mobility tended to increase as the mixing ratio of TCTA or mCP increased, and detailed results are presented in **Fig. 3.9**. Consequently, the current density in the HOD increased more significantly for the device with TCTA compared to the device with mCP which can be attributed to the difference in hole mobility between TCTA and mCP.

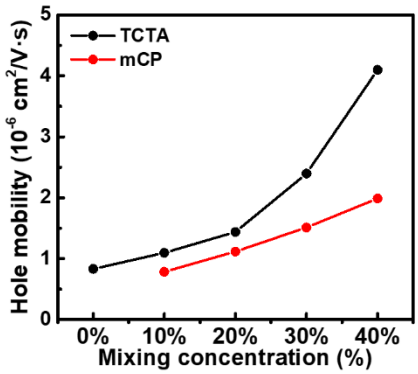

Figure 3.9. Hole mobility as a function of monomer mixing concentration.

An energy level analysis was conducted to determine the effect of mixing TCTA and mCP on the energy level of the HTL. Ultraviolet photoelectron spectroscopy (UPS) was performed by fabricating samples of PVK, PVK:TCTA and PVK:mCP. The secondary electron cut-off and valence band onset regions are illustrated in **Fig. 3.10** and **Fig. 3.11**, respectively. We determined the HOMO through calculations involving the incident photon energy (21.2 eV), the high binding energy cut-off ($E_{\text{cut-off}}$) and the onset energy in valence-band region (E_{onset}). The mathematical representations for this calculation is as follows [33].

$$\text{VBM} = 21.2 - (E_{cut-off} - E_{onset})$$

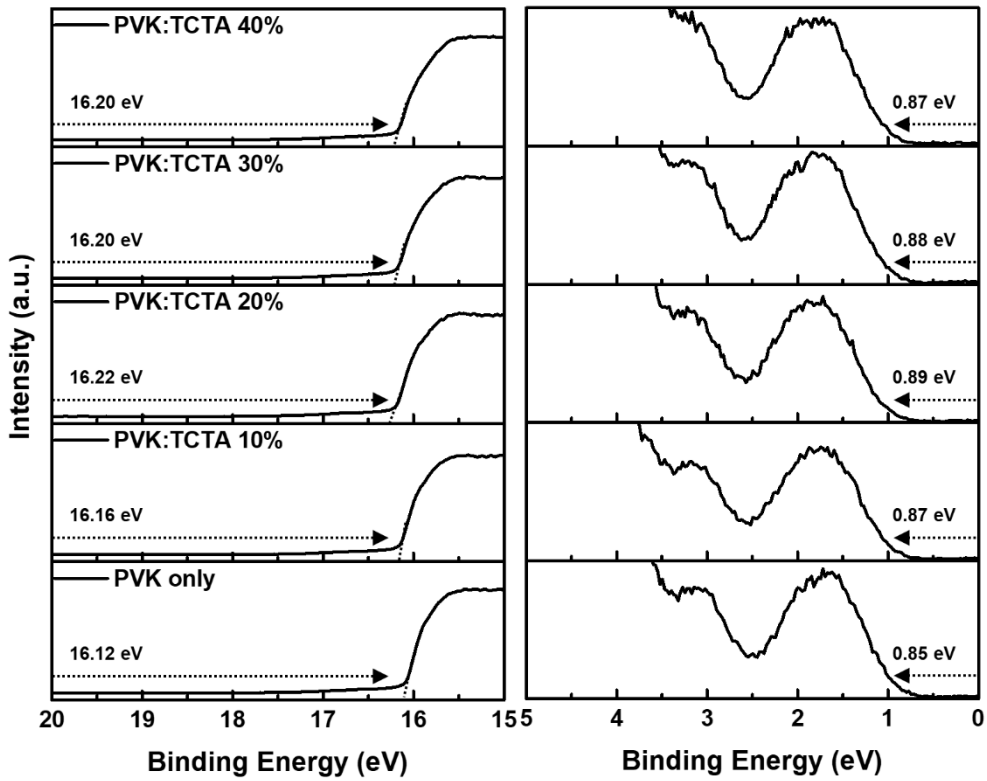

Figure 3.10. UPS spectra of (a) the secondary electron cut-off region and (b) the valence-band edge region for PVK only or PVK:TCTA.

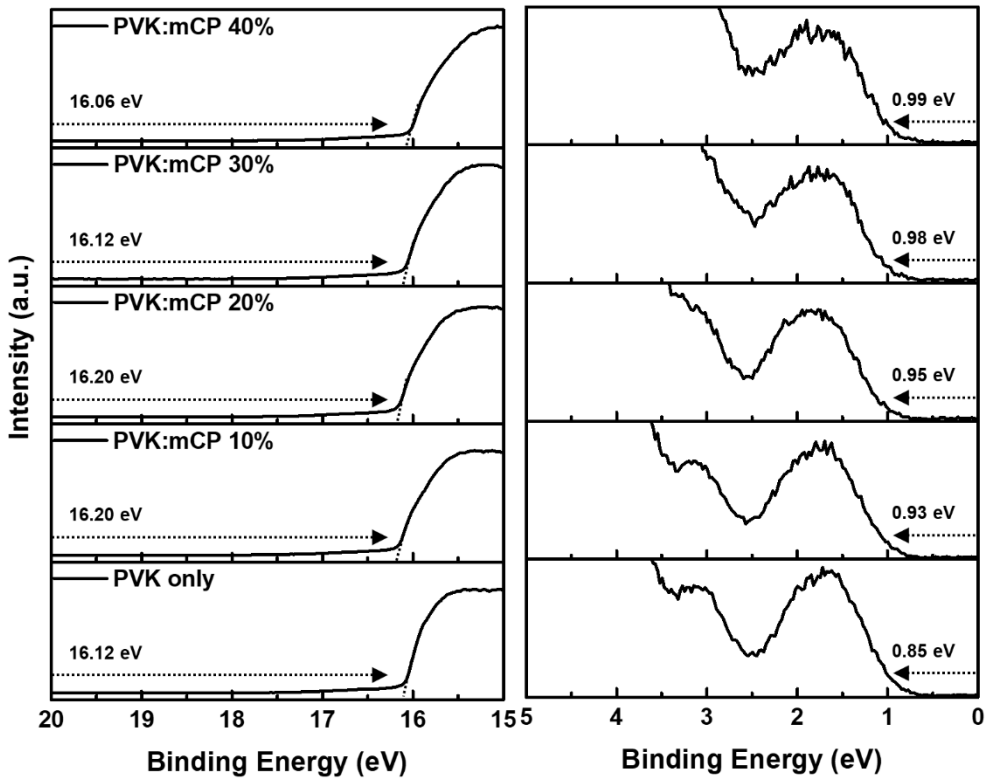

Figure 3.11. UPS spectra of (a) the secondary electron cut-off region and (b) the valence-band edge region for PVK only or PVK:mCP.

Based on the measurement results, the HOMO was calculated to be 5.93 eV for PVK, 5.87 eV for PVK:TCTA 20% and 5.95 eV for PVK:mCP 20%. Hence, when TCTA was mixed with PVK, the energy level was upshifted and the injection barrier to the EML increased. In contrast, for the mCP mixture, the energy level was downshifted, reducing the injection barrier to the EML and consequently changing the direction of smoothing hole injection. The detailed values of the device per condition are illustrated in **Fig. 3.12**. Hole injection into the EML affected both the injection barrier of the HTL/EML interface and also the hole mobility in the HTL. Therefore, despite the increased injection barrier by mixing TCTA, the rapid hole mobility

further strengthened the hole injection of the device containing TCTA compared with the device containing mCP.

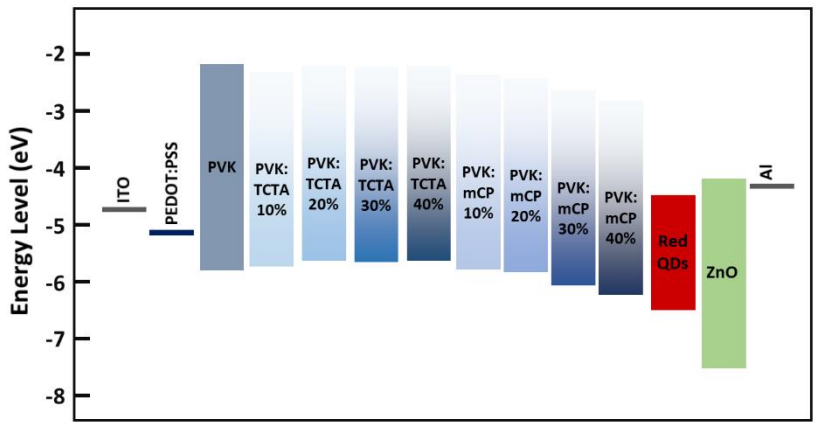

Figure 3.12. Flat-band energy level diagram of different HTLs.

3.3 Conclusion

In this study, we propose a high-efficiency, low-power-driving QLED device structure by mixing two different monomers, TCTA and mCP, with PVK. When a TCTA-mixed HTL was applied to the device, the HTL hole mobility increased and EML hole transport accelerated, which improved the current efficiency and power efficiency by 24% and 52%, respectively. Similarly, using an mCP-mixed HTL, improvements were observed in current efficiency and power efficiency by 20% and 47%, respectively, owing to energy level shifting by the reduction in the injection barrier and increase in hole transport. The proposed fabrication method can enhance the device properties by simply mixing monomers with PVK. Hence, we expect this method to be a simple and yet effective method applicable to the development and fabrication of QLED devices for application in mobile devices with high efficiency and low power consumption.

References

1. J. Kwak, W. K. Bae, D. Lee, I. Park, J. Lim, M. Park, H. Cho, H. Woo, D. Y. Yoon, K. Char, S. Lee, and C. Lee, "Bright and Efficient Full-Color Colloidal Quantum Dot Light-Emitting Diodes Using an Inverted Device Structure," *Nano Lett*. **12**, 2362–2366 (2012).

2. W. Sun, L. Xie, X. Guo, W. Su, and Q. Zhang, "Photocross-Linkable Hole Transport Materials for Inkjet-Printed High-Efficient Quantum Dot Light-Emitting Diodes," *ACS Appl. Mater. Interfaces* **12**, 58369–58377 (2020).

3. L. Xie, X. Xiong, Q. Chang, X. Chen, C. Wei, X. Li, M. Zhang, W. Su, and Z. Cui, "Inkjet-Printed High-Efficiency Multilayer QLEDs Based on a Novel Crosslinkable Small-Molecule Hole Transport Material," *Small* **15**, 1900111 (2019).

4. Y.-Q.-Q. Yi, J. Yang, L. Xie, Y. Liu, W. Su, and Z. Cui, "Linear cross-linkers enabling photothermally cured hole transport layer for high-performance quantum dots light-emitting diodes with ultralow efficiency roll-off," *Chem. Eng. J.* **439**, 135702 (2022).

5. Y.-Q.-Q. Yi, D. Qi, H. Wei, L. Xie, Y. Chen, J. Yang, Z. Hu, Y. Liu, X. Meng, W. Su, and Z. Cui, "Molecular Design of Diazo Compound for Carbene-Mediated Cross-Linking of Hole-Transport Polymer in QLED with Reduced Energy Barrier and Improved Charge Balance," *ACS Appl. Mater. Interfaces* **14**, 39149–39158 (2022).

6. W. Sun, Y. Deng, Y. Jin, X. Guo, and Q. Zhang, "Solvent Resistant Hole-Transporting Thin Films via Diacetylene Cross-Linking and Their

Applications in Solution-Processed QLEDs," *ACS Appl. Polym. Mater.* **2**, 3274–3281 (2020).

7. Y. Zou, Y. Liu, M. Ban, Q. Huang, T. Sun, Q. Zhang, T. Song, and B. Sun, "Crosslinked conjugated polymers as hole transport layers in high-performance quantum dot light-emitting diodes," *Nanoscale Horiz.* **2**, 156–162 (2017).

8. P. Tang, L. Xie, X. Xiong, C. Wei, W. Zhao, M. Chen, J. Zhuang, W. Su, and Z. Cui, "Realizing 22.3% EQE and 7-Fold Lifetime Enhancement in QLEDs via Blending Polymer TFB and Cross-Linkable Small Molecules for a Solvent-Resistant Hole Transport Layer," *ACS Appl. Mater. Interfaces* **12**, 13087–13095 (2020).

9. S.-W. Chao, W.-S. Chen, W.-Y. Hung, Y.-Y. Chen, Y.-M. Lin, K.-T. Wong, and P.-T. Chou, "Cross-linkable hole transporting layers boost operational stability of high-performance quantum dot light-emitting device," *Org. Electron.* **71**, 206–211 (2019).

10. L. Xie, J. Yang, W. Zhao, Y. Yi, Y. Liu, W. Su, Q. Li, W. Lei, and Z. Cui, "High-Performance Inkjet-Printed Blue QLED Enabled by Crosslinked and Intertwined Hole Transport Layer," *Adv. Opt. Mater.* **10**, 2200935 (2022).

11. J. Chen, D. Song, S. Zhao, B. Qiao, W. Zheng, and Z. Xu, "Highly efficient all-solution processed blue quantum dot light-emitting diodes based on balanced charge injection achieved by double hole transport layers," *Org. Electron.* **94**, 106169 (2021).

12. J. H. Hwang, J. Kim, B. J. Kim, M. Park, Y. W. Kwon, M. An, D. Y. Shin, J. M. Jeon, J. Y. Kim, W. Lee, J. Lim, and D. Lee, "Hole injection of quantum dot light-emitting diodes facilitated by multilayered hole transport layer," *Appl. Surf. Sci.* **558**, 149944 (2021).

13. H. Chen, K. Ding, L. Fan, W. Liu, R. Zhang, S. Xiang, Q. Zhang, and L. Wang, "All-Solution-Processed Quantum Dot Light Emitting Diodes Based on Double Hole Transport Layers by Hot Spin-Coating with Highly Efficient and Low Turn-On Voltage," *ACS Appl. Mater. Interfaces* **10**, 29076–29082 (2018).

14. Y. R. Park, J. H. Doh, K. Shin, Y. S. Seo, Y. S. Kim, S. Y. Kim, W. K. Choi, and Y. J. Hong, "Solution-processed quantum dot light-emitting diodes with PANI:PSS hole-transport interlayers," *Org. Electron.* **19**, 131–139 (2015).

15. Y. Liu, C. Jiang, C. Song, J. Wang, L. Mu, Z. He, Z. Zhong, Y. Cun, C. Mai, J. Wang, J. Peng, and Y. Cao, "Highly Efficient All-Solution Processed Inverted Quantum Dots Based Light Emitting Diodes," *ACS Nano* **12**, 1564–1570 (2018).

16. W. Zheng, D. Song, S. Zhao, B. Qiao, Z. Xu, J. Chen, P. Wang, and Y. Liang, "All-solution processed inverted QLEDs with double hole transport layers and thermal activated delay fluorescent dopant as energy transfer medium," *Org. Electron.* **77**, 105544 (2020).

17. S.-H. Song, J.-I. Yoo, H.-B. Kim, Y.-S. Kim, S. Soo Kim, and J.-K. Song, "Hole injection improvement in quantum-dot light-emitting diodes using bi-layered hole injection layer of PEDOT:PSS and V_2O_x" *Opt. Laser Technol.* **149**, 107864 (2022).

18. M. Yang, Q. Zhang, W. Zhang, Z. Hao, Y. Qin, X. Hai, F. Li, D. Zhou, and Y. Zhang, "Enhanced hole transport by doping of a lewis acid to Poly(9-vinylcarbazole) for high efficient quantum dot light-emitting diodes," *Org. Electron.* **85**, 105875 (2020).

19. Y.-L. Shi, F. Liang, Y. Hu, X.-D. Wang, Z.-K. Wang, and L.-S. Liao, "High-efficiency quantum dot light-emitting diodes employing lithium salt doped poly(9-vinlycarbazole) as a hole-transporting layer," *J. Mater. Chem. C* **5**, 5372–5377 (2017).

20. J. Pan, J. Chen, Q. Huang, L. Wang, and W. Lei, "A highly efficient quantum dot light emitting diode via improving the carrier balance by modulating the hole transport," *RSC Adv.* **7**, 43366–43372 (2017).

21. S.-K. Kim, H. Yang, and Y.-S. Kim, "Control of carrier injection and transport in quantum dot light emitting diodes (QLEDs) via modulating Schottky injection barrier and carrier mobility," *J. Appl. Phys.* **126**, 185702 (2019).

22. B. Li, Y. Fang, P. Bai, Y. Wang, J. Li, B. Xiao, and Y. Wang, "Effect of PVK mixed TAPC as hole transport layers on device performance of red quantum-dot light-emitting diodes," *J. Lumin.* **247**, 118871 (2022).

23. Y. Fang, P. Bai, J. Li, B. Xiao, Y. Wang, and Y. Wang, "Highly Efficient Red Quantum Dot Light-Emitting Diodes by Balancing Charge Injection and Transport," *ACS Appl. Mater. Interfaces* **14**, 21263–21269 (2022).

24. Q. Huang, J. Pan, Y. Zhang, J. Chen, Z. Tao, C. He, K. Zhou, Y. Tu, and W. Lei, "High-performance quantum dot light-emitting diodes with hybrid hole transport layer via doping engineering," *Opt. Express* **24**, 25955 (2016).

25. Y. Zhao, L. Chen, J. Wu, X. Tan, Z. Xiong, and Y. Lei, "Composite Hole Transport Layer Consisting of High-Mobility Polymer and Small Molecule With Deep-Lying HOMO Level for Efficient Quantum Dot Light-Emitting Diodes," *IEEE Electron Device Lett*. **41**, 80–83 (2020).

26. X. Lin, X. Wu, J. Zheng, H. Rui, Z. Zhang, Y. Hua, and S. Yin, "Enhanced Performance of Green Perovskite Quantum Dots Light-Emitting Diode Based on Co-Doped Polymers as Hole Transport Layer," *IEEE Electron Device Lett*. **40**, 1479–1482 (2019).

27. B. S. Kim and J. Y. Lee, "Engineering of Mixed Host for High External Quantum Efficiency above 25% in Green Thermally Activated Delayed Fluorescence Device," *Adv. Funct. Mater.* **24**, 3970–3977 (2014).

28. S. Noh, C. K. Suman, Y. Hong, and C. Lee, "Carrier conduction mechanism for phosphorescent material doped organic semiconductor," *J. Appl. Phys.* **105**, 033709 (2009).

29. Y. Tao, C. Yang, and J. Qin, "Organic host materials for phosphorescent organic light-emitting diodes," *Chem. Soc. Rev.* **40**, 2943 (2011).

30. Y. Tsuchiya, N. Nakamura, S. Kakumachi, K. Kusuhara, C.-Y. Chan, and C. Adachi, "A convenient method to estimate the glass transition temperature of small organic semiconductor materials," *Chem. Commun.* **58**, 11292–11295 (2022).

31. V. Wood, M. J. Panzer, J.-M. Caruge, J. E. Halpert, M. G. Bawendi, and V. Bulović, "Air-Stable Operation of Transparent, Colloidal Quantum Dot Based LEDs with a Unipolar Device Architecture," *Nano Lett.* **10**, 24–29 (2010).

32. A. Castan, H.-M. Kim, and J. Jang, "All-Solution-Processed Inverted Quantum-Dot Light-Emitting Diodes," *ACS Appl. Mater. Interfaces* **6**, 2508–2515 (2014).

33. J.-H. Kim, C.-Y. Han, K.-H. Lee, K.-S. An, W. Song, J. Kim, M. S. Oh, Y. R. Do, and H. Yang, "Performance Improvement of Quantum Dot-Light-

Emitting Diodes Enabled by an Alloyed ZnMgO Nanoparticle Electron Transport Layer," *Chem. Mater.* **27**, 197–204 (2015).

Chapter 4

Controlling Electron Injection for Improving Charge Balance of Quantum Dot Light-emitting Diodes

4.1 Introduction

In Chapter 3, we dealt with the study on enhancing hole injection to improve the charge balance of QLEDs. In this chapter, we will describe the research on suppressing excess electrons. Excess electrons are known to increase the probability of non-radiative recombination due to charge imbalance and adversely affect the device's reliability by damaging the EML and HTL. Therefore, suppressing excess electrons that are injected into the EML of QLEDs is essential for improving device characteristics [1-3].

As summarized in **Fig. 4.1**, a wide variety of studies have been conducted on suppressing excess electrons in QLEDs. The methods for suppressing excess electrons in QLEDs can broadly be divided into two types. The first method changes the composition of the ETL [4-15], and the second method inserts an interlayer that can function as the injection barrier for electrons at the interface between the EML and ETL [16-23]. In addition, various studies have been conducted to control the characteristics of ETL by blending polymers [24-26] or monomers [27] into ETL or passivating oxygen vacancy through surface treatment [28, 29].

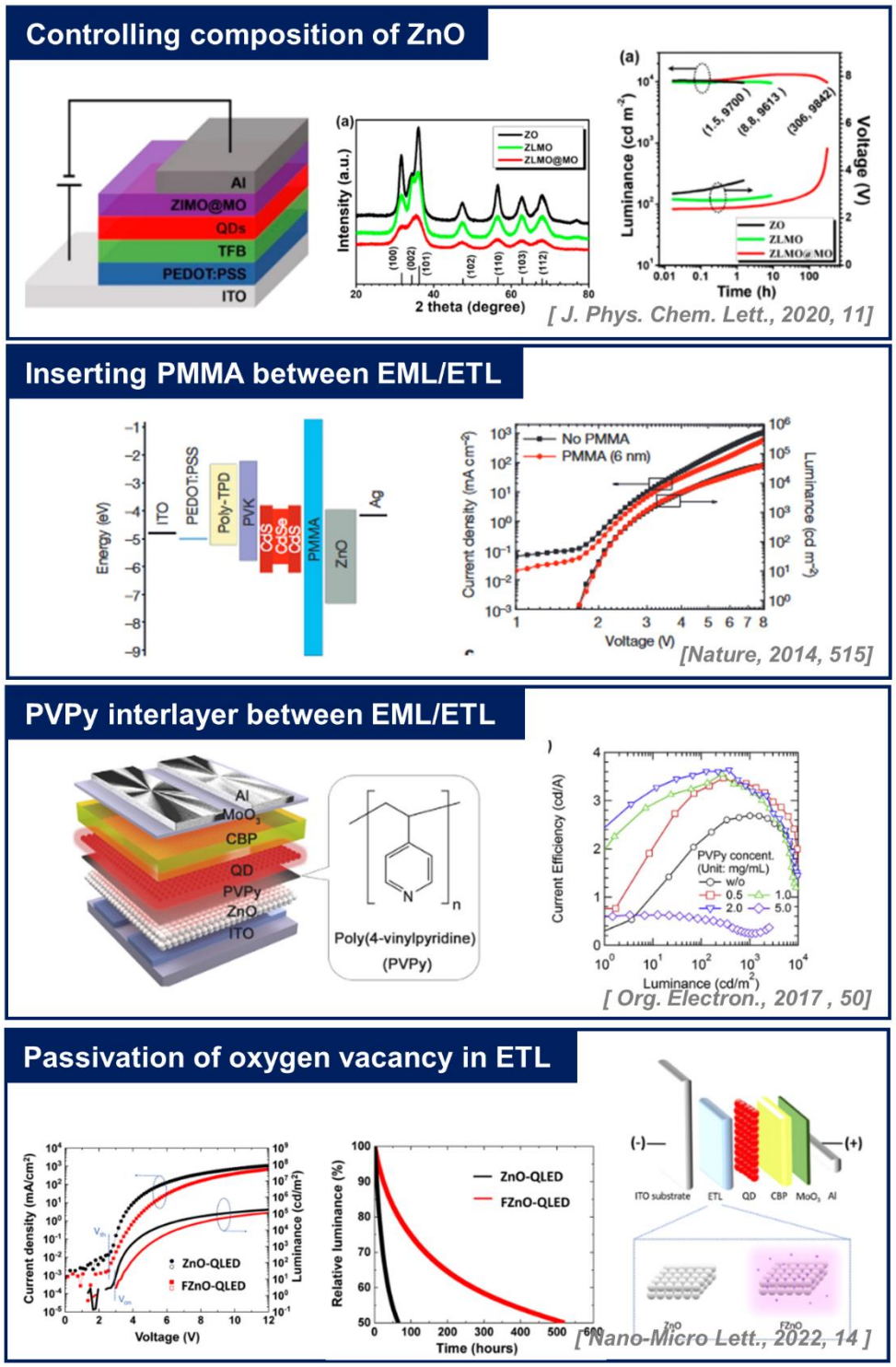

Figure 4.1. Various studies on suppression electron injection in QLEDs [11, 16, 19, 29].

In this chapter, we utilized both the application of the interlayer and controlling the mobility of the ETL to control excess electrons. A polyethylenimine (PEI) with a high LUMO and a very thin thickness (~5 nm) was designed to be applied to the device to function as the electron injection barrier. ZnO, which is the ETL, was doped with a small amount of LiQ to reduce the mobility of the ETL. (8-Quinolinolato)lithium (LiQ) is widely used as an n-type dopant in OLEDs, and it is a material that can enhance electron injection due to the weak bonding between Li and ligand. It was deposited as a thin film with a thickness of less than or equal to 1 nm and used as the EIL at the interface between the ETL and cathode. It can also be applied as a mixed ETL by mixing organic ETL materials like TPBi and BPhen [29]. However, this material is an insulator with very low mobility. Hence, it was used as a dopant in this study to lower the electron mobility of ZnO. **Figure 4.2(a)** shows the molecular structures of PEI and LiQ, and **Figure 4.2(b)** shows the flat-band energy level diagram. The detailed properties of the materials are summarized in **Table 4.1** [9, 18, 30]. The values reported in previous research papers were used as the HOMO and LUMO values of each material [9, 31]. Moreover, the two methods mentioned above for suppressing the injection of electrons were evaluated individually as well as in combination.

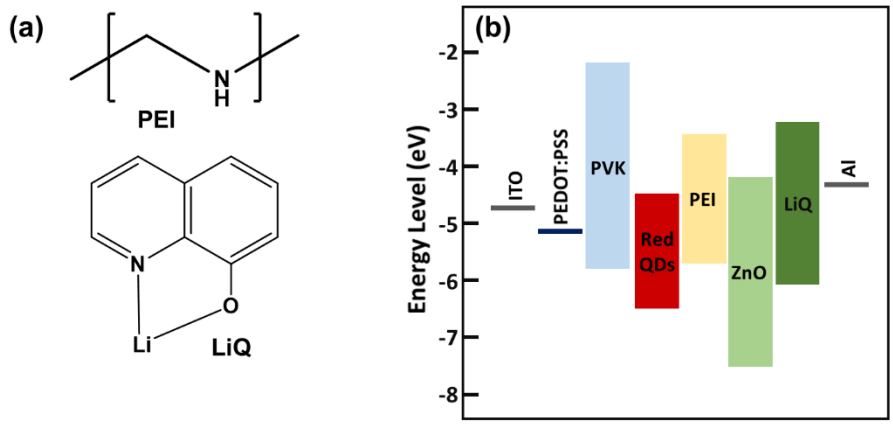

Figure 4.2. (a) Molecular structures of PEI and LiQ. (b) Energy level diagram for various layers of the QLEDs.

Device	ZnO	PEI	LiQ
HOMO (eV)	-7.4	-6.9	-5.7
LUMO (eV)	-3.9	-3.4	-3.1
Electron mobility ($cm^2/V{\cdot}s$)	10^{-3}~10^{-4}	Insulator	Insulator

Table 4.1. Physical properties of used materials [9, 18, 30].

4.2 Result and Discussion

4.2.1 PEI interlayer

First, the device was fabricated by incorporating a high LUMO polyethylenimine (PEI) as the electron injection barrier. **Figure 4.3** illustrates the characteristics of the fabricated device. As depicted in **Fig. 4.3**, the current density exhibits a declining trend with increasing applied voltage, while the luminance diminishes as the interlayer is introduced. The reduction in current density and the rise in turn-on voltage indicate the suppression of electron injection upon interlayer application. However, the maximum current efficiency improved with the implementation of the PEI interlayer. Specifically, the current efficiency reached 7.31 cd/A, representing a 20% increase compared to the current efficiency of the reference device, which was 6.09 cd/A. The interlayer application led to an enhancement in current efficiency across all current densities. Notably, the most significant improvements in device characteristics were observed in the low-field region (~1 mA/cm^2), while the efficiency tended to converge with that of the reference device in the high-field region. This suggests that the PEI interlayer effectively functions as an injection barrier in the low-field region due to its minimal thickness, but exhibits reduced efficacy as an injection barrier in the high-field region, where electrons can tunnel through the interlayer. The electron injection suppression can be further elucidated through the analysis of electron-only devices (EOD) consisting of ITO/ZnO (35 nm)/EML (20 nm)/interlayer (0 or 5 nm)/ETLs (35 nm)/LiF (1 nm)/Al (50 nm). **Figure**

4.3(d) illustrates a decrease in current density across all voltage ranges when the PEI interlayer is introduced, compared to the reference device. However, similar to the full device characteristics, the current density experiences a significant decline in the low-field region (~1 mA/cm^2), gradually converging to the reference device curve in the high-field region (1~ mA/cm^2). The detailed device characteristics under different conditions are summarized in **Table 4.2**.

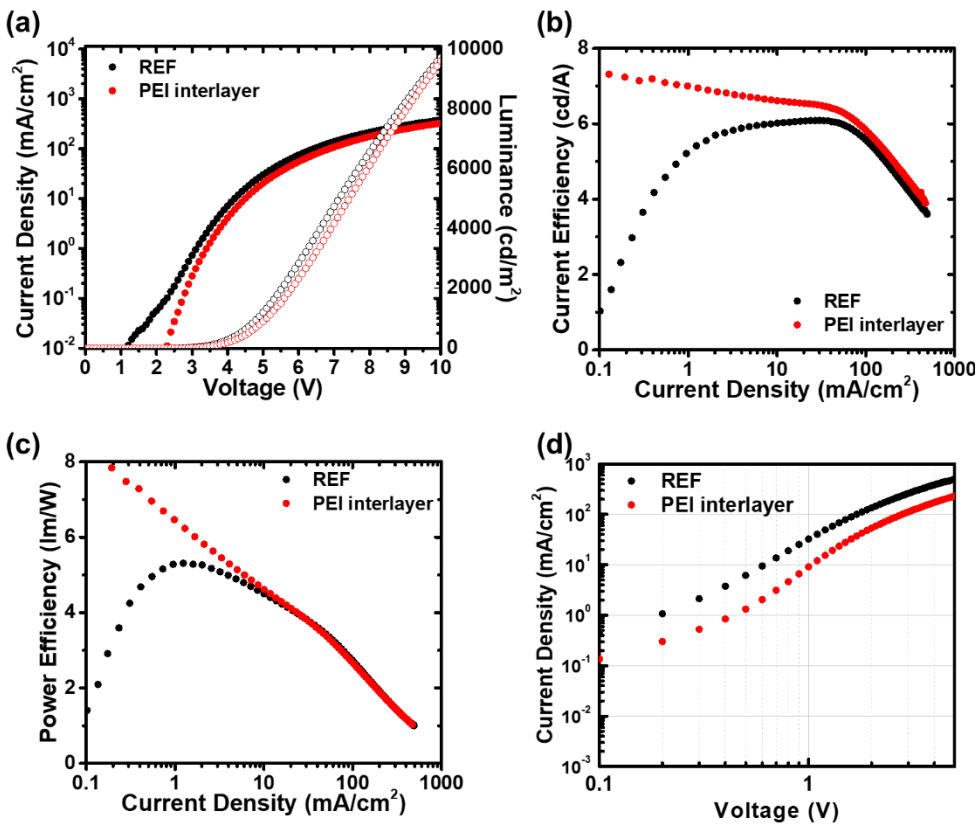

Figure 4.3. Electroluminescence (EL) performance of the QLEDs without or with PEI interlayer. (a) Current density-voltage-luminance (*J-V-L*) characteristics. (b) Current efficiency-current density characteristics. (c) Power efficiency-current density characteristics. (d) Current density-voltage (*J-V*) characteristics of EODs.

Device	V_{on} (V)	V_d (V)	Max CE (cd/A)	Max PE (lm/W)	λ_{max} (nm)	CIE coordinate (x,y)
Ref	2.3	4.8	6.09	5.31	627	(0.68, 0.32)
PEI interlayer	2.4	5.0	7.31	8.61	627	(0.68, 0.32)

[a] V_{on} is the turn-on voltage corresponding to 1 cd/m^2, and V_d is the driving voltage corresponding to 1000 cd/m^2.

Table 4.2. Performance summary of QLEDs without or with PEI interlayer.

Since it is known that the decline of the operational lifetime of typical QLED devices is caused by excess electrons [32], we checked how the room-temperature operational lifetime changed for the device in which excess electrons were controlled by the interlayer. The room-temperature operational lifetime of the device was evaluated under the luminance condition of 300 nits. As shown in Figure 4.4, the evaluation result shows that T_{50} (the operational lifetime to reach 50 % of the initial luminance) is about 15 hours, regardless of whether or not the PEI interlayer has been applied. Hence, the operational lifetime did not improve, and the increase in the driving voltage due to operation was at the same level.

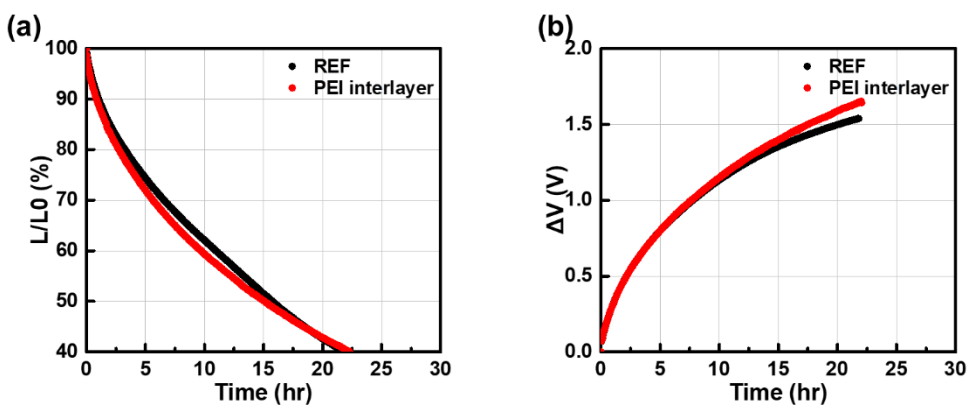

Figure 4.4. (a) Luminance decay vs time and (b) driving voltage increase vs time of the QLEDs without or with PEI interlayer.

4.2.2 ZnO:LiQ ETL

Next, we evaluated the characteristics of the device to which ZnO:LiQ ETL was applied and in which the injection of electrons was suppressed by controlling the mobility of the ETL. As shown in **Figure 4.5**, when LiQ is mixed with ZnO and applied as the ETL, the *J-V* curve is shifted to the back , the turn-on voltage increases, the current density at the applied voltage decreases, and the luminance and current efficiency decrease. Similar to the earlier PEI interlayer evaluation result, the decrease in the current density and increase in the turn-on voltage indicate that electron injection is suppressed by applying the LiQ-doped ETL. Moreover, the device characteristics exhibited changes based on the LiQ doping ratio. When ZnO is doped with LiQ at 2%, 3%, and 5%, the current efficiency declines by 4%, 8%, and 13%, respectively, compared to the reference device. This suggests that the degradation of device characteristics becomes more pronounced with higher levels of LiQ doping. When the doped ETL was implemented, the current efficiency experienced a decrease across all current densities, particularly in the low-field region (~1 mA/cm^2), implying that the device operates through a distinct mechanism compared to the interlayer. To gain further insights into the behavior of electrons within the LiQ-doped ETL, we fabricated an electron-only device (EOD) and examined its characteristics. In the case of the device utilizing LiQ-doped ETL, the current density exhibited a decrease compared to the reference device, with a consistent decline observed in all regions, in contrast to the PEI interlayer device. Furthermore, the impact of LiQ concentration on device characteristics was also observed in the EOD. A

comprehensive summary of the device characteristics based on different conditions is provided in **Table 4.3**.

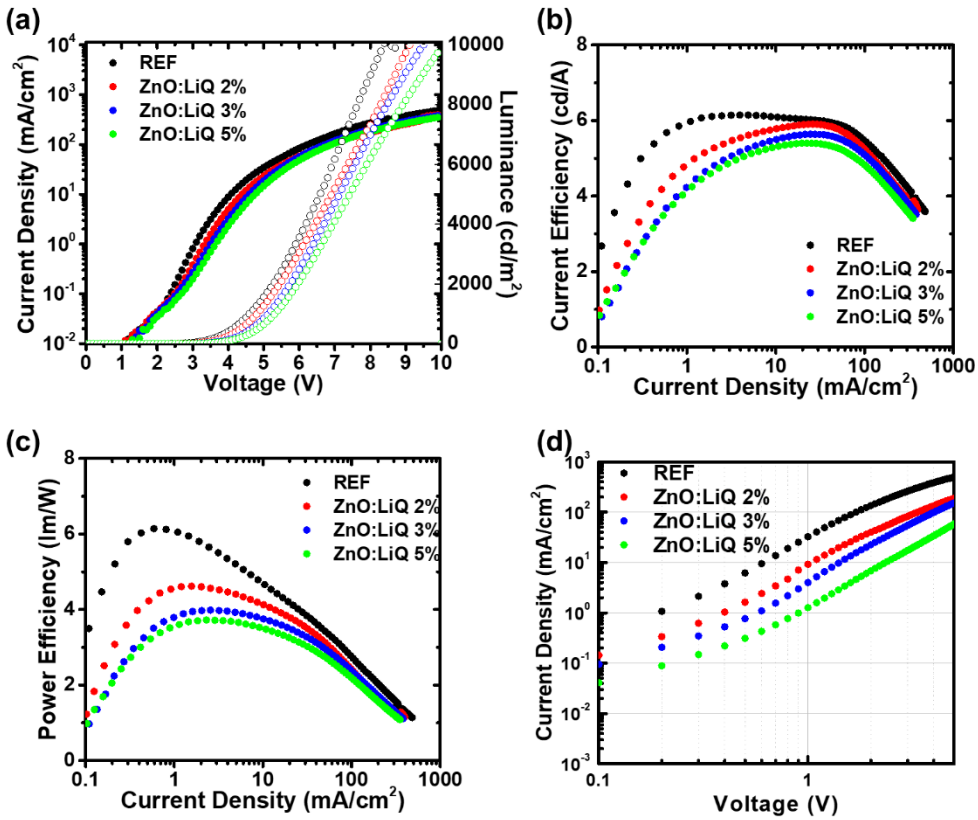

Figure 4.5. Electroluminescence (EL) performance of the QLEDs with ZnO or ZnO:LiQ ETLs. (a) Current density-voltage-luminance (*J-V-L*) characteristics. (b) Current efficiency-current density characteristics. (c) Power efficiency-current density characteristics. (d) Current density-voltage (*J-V*) characteristics of EODs.

Device	V_{on} (V)	V_d (V)	Max CE (cd/A)	Max PE (lm/W)	λ_{max} (nm)	CIE coordinate (x,y)
Ref	2.2	4.6	6.15	6.15	627	(0.68, 0.32)
ZnO:LiQ 2%	2.5	4.8	5.91	4.62	627	(0.68, 0.32)
ZnO:LiQ 3%	2.6	5.1	5.64	3.99	627	(0.68, 0.32)
ZnO:LiQ 5%	2.7	5.3	5.40	3.72	628	(0.68, 0.32)

[a] V_{on} is the turn-on voltage corresponding to 1 cd/m^2, and V_d is the driving voltage corresponding to 1000 cd/m^2.

Table 4.3. Performance summary of QLEDs with various ETLs.

The room-temperature operational lifetime of the device was evaluated, focusing on the control of excess electrons through the LiQ-doped ETL. Similar to the previous experiment, the evaluation of the device's room-temperature operational lifetime was conducted under a luminance condition of 300 nits. As illustrated in **Fig. 4.6**, the reference device (ZnO-only device) exhibited a T_{50} value of approximately 12 hours. However, when the ZnO:LiQ doped ETL was applied, the operational lifetime of the device increased to 18, 22, and 26 hours, respectively, depending on the concentration of LiQ. The graph depicting the rise in driving voltage over operating time reveals a marginal increase in the driving voltage for devices with longer room-temperature operational lifetimes.

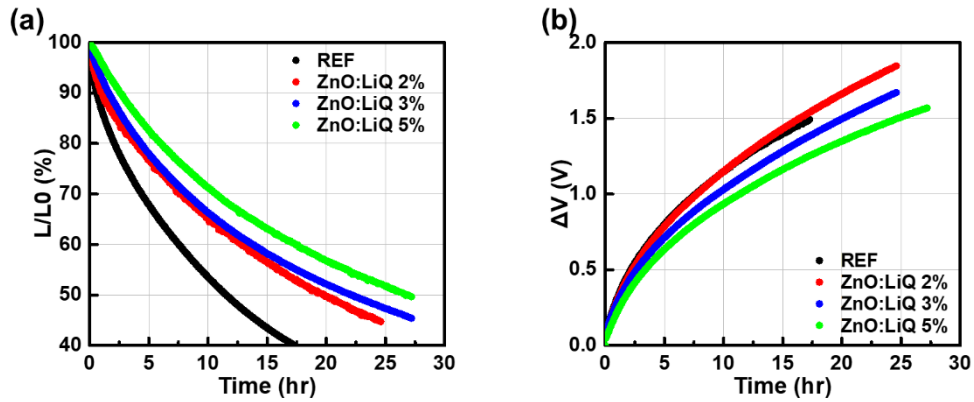

Figure 4.6. (a) Luminance decay vs time and (b) driving voltage increase vs time of the QLEDs with ZnO or ZnO:LiQ ETLs.

In order to determine why the behavior of the device is different depending on whether the PEI interlayer or mixed-ETL is applied, we conducted the time-resolved photoluminescence (TrPL) measurements on five samples: QDs, QDs/ZnO, QDs/PEI/ZnO, QDs/ZnO:LiQ, and QDs/PEI/ZnO:LiQ. As illustrated in **Fig 4.7(a)**, the QD-only sample exhibited the longest PL decay time. However, the PL decay time decreased for the QD/ZnO sample, which shares the same stacked structure as the reference device of QLEDs This decrease indicates that the excitons formed in the EML were quenched by the traps in the metal oxide. Interfacial charge-transfer at the EML-ETL interface, known to induce exciton quenching, results in QD charging and non-radiative Auger recombination, thereby degrading device characteristics.

Compared to the reference sample with ZnO ETL, the PL decay time increased when the PEI interlayer was employed. Conversely, when the LiQ-doped ETL was utilized, the PL decay time decreased compared to the reference device. Moreover, when both the PEI interlayer and ZnO:LiQ ETL

were applied together, the PL decay time was longer than that of ZnO:LiQ alone. To facilitate a quantitative comparison, τ_{av} (average decay time) was determined using the following equation [7].

$$\tau_{av} = \frac{A_1\tau_1^2 + A_2\tau_2^2}{A_1\tau_1 + A_2\tau_2}$$

In the above equation, τ_i denotes the time components, and A_i denotes the corresponding weight. The electron transfer rate, k_{ET}, was calculated with τ_{av} extracted using the above equation. The detailed characteristics for each condition are summarized in **Table 4.4**.

$$k_{ET} = \frac{1}{\tau_{av(QDs/ETLs)}} - \frac{1}{\tau_{av(QDs)}}$$

In **Fig. 4.7(b)**, the plots of τ_{av} and k_{ET} for QDs with different ETLs are presented. When the PEI interlayer is applied to the reference device with a k_{ET} value of 6.12×10^7 /s, the charge transfer process between the QDs and metal oxide weakens, resulting in a reduced k_{ET} value of 5.56×10^7 /s. This leads to an increase in the exciton lifetime. Conversely, when the LiQ-doped ETL is utilized, the charge transfer process between the QDs and ETL becomes more efficient, resulting in an enhanced k_{ET} value of 6.92×10^7 /s. Consequently, the exciton lifetime decreases, leading to the degradation of device characteristics.

Energy transfer at the QD/metal oxide interface is known to occur more actively due to the small energy offset between each layer. Therefore, the insertion of a PEI interlayer at the EML/ETL interface can impede the transfer of excited electrons. As a result, the PL decay time is prolonged, and radiative recombination occurs more efficiently in the EML [7, 15].

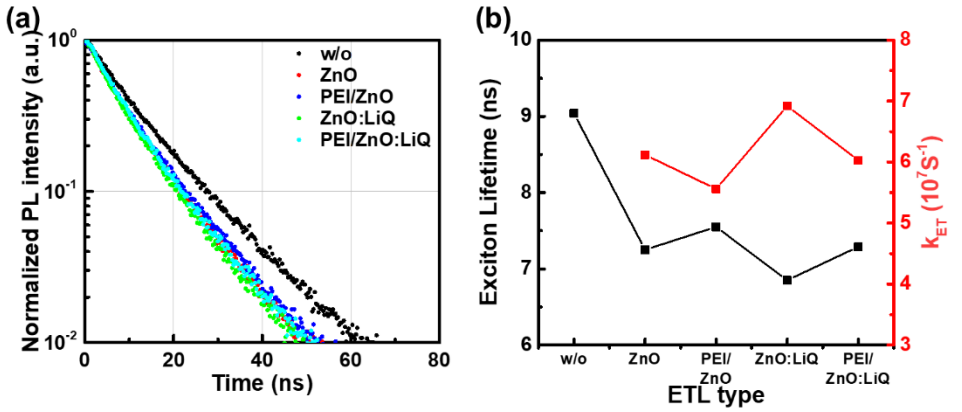

Figure 4.7. (a) Time-resolved PL decay curves of different samples, QDs, QDs/ZnO, QDs/PEI/ZnO, QDs/ZnO:LiQ and QDs/PEI/ZnO:LiQ. (b) Exciton lifetime and electron transfer rate as functions of different ETLs.

ETL type	w/o	ZnO	PEI/ZnO	ZnO:LiQ	PEI/ZnO:LiQ
τ_1 (ns) / A_1 (%)	5.45 / 58.6	4.65 / 66.4	4.46 / 56.0	4.26 / 62.8	5.28 / 81.9
τ_2 (ns) / A_2 (%)	11.45 / 41.4	9.70 / 33.6	9.41 / 44.0	8.94 / 37.2	11.47 / 18.1
Exciton lifetime (ns)	9.04	7.25	7.55	6.85	7.29
k_{ET} ($10^7 s^{-1}$)	-	6.12	5.56	6.92	6.03
R^2 (COD)	0.9995	0.9996	0.9996	0.9995	0.9993

Table 4.4. Exciton lifetime and electron transfer rate as functions of different ETLs.

To discern more clearly the cause of the different charge transfer processes for each ETL condition, the SCLC analysis was performed separately for the full device and EOD. The *J-V* curve of a semiconducting device can be divided into Ohmic current ($J \propto V$), trap-limited space charge limited current (t-SCLC, $J \propto V^{1\sim2}$), trap-filled limited current (TFL, $J \propto V^{2\sim100}$), and space charge limited current (SCLC, $J \propto V^2$), according to the relation between J and V [9].

First, **Figure 4.8** shows the *J-V* relation for each ETL condition. Although the experimental results do not perfectly conform to the typical *J-V*

relation, the different regions are clearly distinguishable. According to **Fig. 4.8 (a)**, the *J-V* curve of the reference device has an exponent of 1.0 under 1.3 V, 2.8 under 2.2 V, 8.5 under 4.4 V, and 3.5 over 4.4 V. In the ohmic region, no significant condition-specific differences or anomalies were observed. However, in the case of the device to which the PEI interlayer was applied, the t-SCLC region could not be clearly distinguished when transitioning from the ohmic current region to the trap-filled limited current region. The most noticeable finding from the SCLC analysis of the devices is the value of the exponent of the devices at TFL. When the PEI interlayer was applied, the value of the exponent at TFL was 10.1, which was considerably larger than the reference value of 8.5. Furthermore, in the case of devices to which the ZnO:LiQ ETL was applied, it was found that the value of the exponent decreased gradually to 8.1, 7.8, and 7.2, depending on the doping concentration. This result indicates that when the PEI interlayer is applied, the electron trap sites in the ETL are filled much faster and more efficiently [24]. On the other hand, in the case of ZnO:LiQ, the value of the exponent decreased, which means that as the concentration of LiQ increases, more charges are required to fill the electron trap sites.

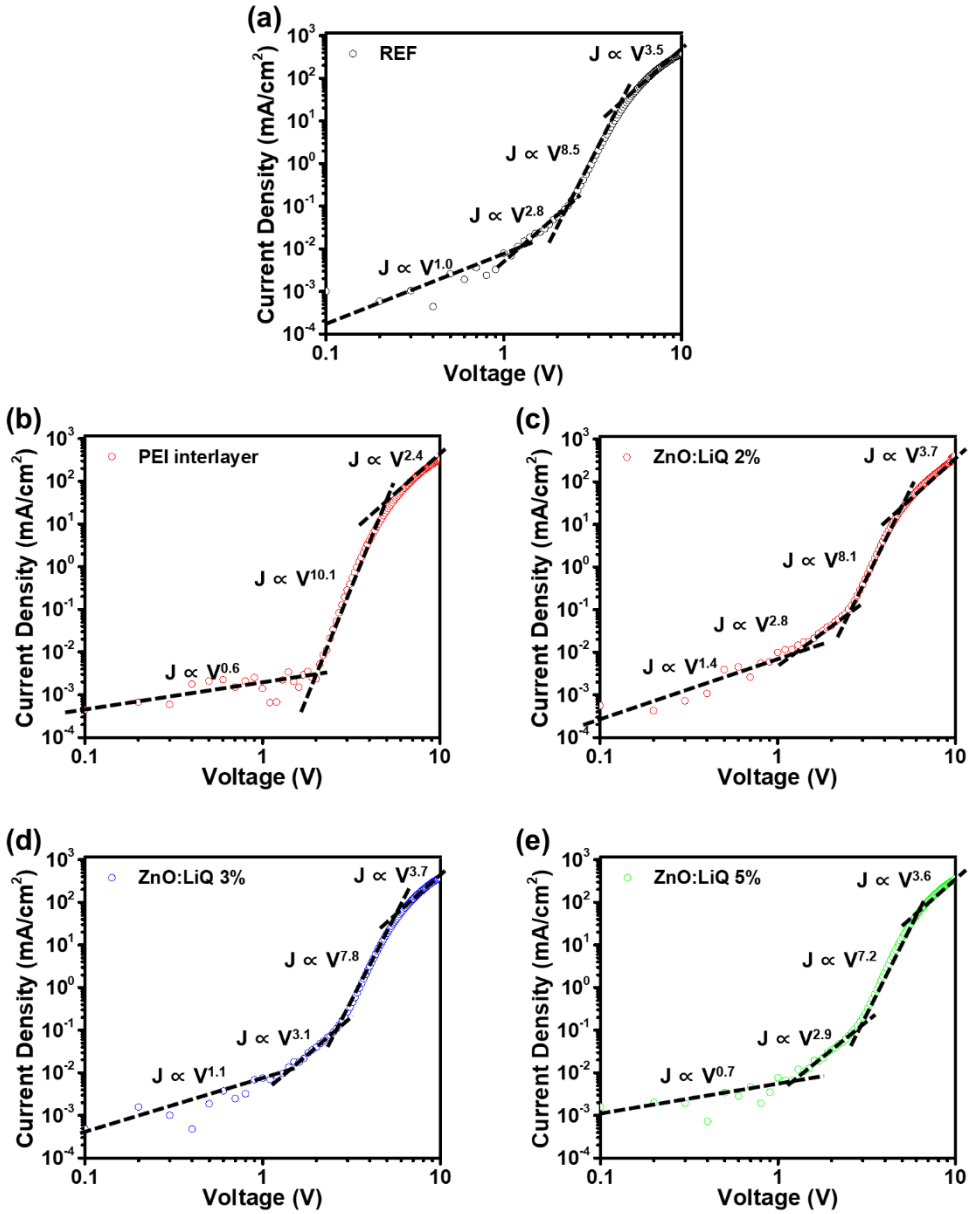

Figure 4.8. Current density-voltage (*J-V*) curve of full devices with (a) ZnO. (b) PEI/ZnO. (c) ZnO:LiQ 2%. (d) ZnO:LiQ 3%. and (e) ZnO:LiQ 5%.

In addition to the full device, the SCLC analysis was also performed on the EOD in the same manner. **Figure 4.9** shows both the *J-V* curve and *J-V* relation of the EOD fabricated for each condition. In accordance with the purpose of the experiment for suppressing electron injection, the current density decreased in both cases where the PEI interlayer and ZnO:LiQ ETL were applied. To check the effect of the electron trap for each condition, the V_{TFL} was plotted on the graph. V_{TFL} is defined as the voltage at which the transition from TFL to SCLC occurs, and it can be calculated using the equation below [9].

$$V_{TFL} = \frac{qH_b d^2}{2\varepsilon\varepsilon_0}$$

Here, q denotes the charge of the carrier, H_b denotes the charge trap density, and d denotes the thickness of the layers. In addition, ε denotes the dielectric constant of the material, and ε_0 denotes the dielectric constant of the vacuum (8.85×10^{-14} C/V·cm). According to the above equation, the V_{TFL} is determined by the density of the charge traps when the thickness of the active layer is fixed. When the V_{TFL} of the reference was 2.0 V, the V_{TFL} of the PEI interlayer condition was 2.0 V; hence, it was same as that of the reference. However, the V_{TFL} of the device to which the ZnO:LiQ ETL was applied increased significantly to 2.8 V, 5.4 V, and >10 V according to the doping ratio. Based on this result, we could infer that electron trap sites, such as oxygen vacancy in the ZnO ETL, increased significantly when LiQ was doped.

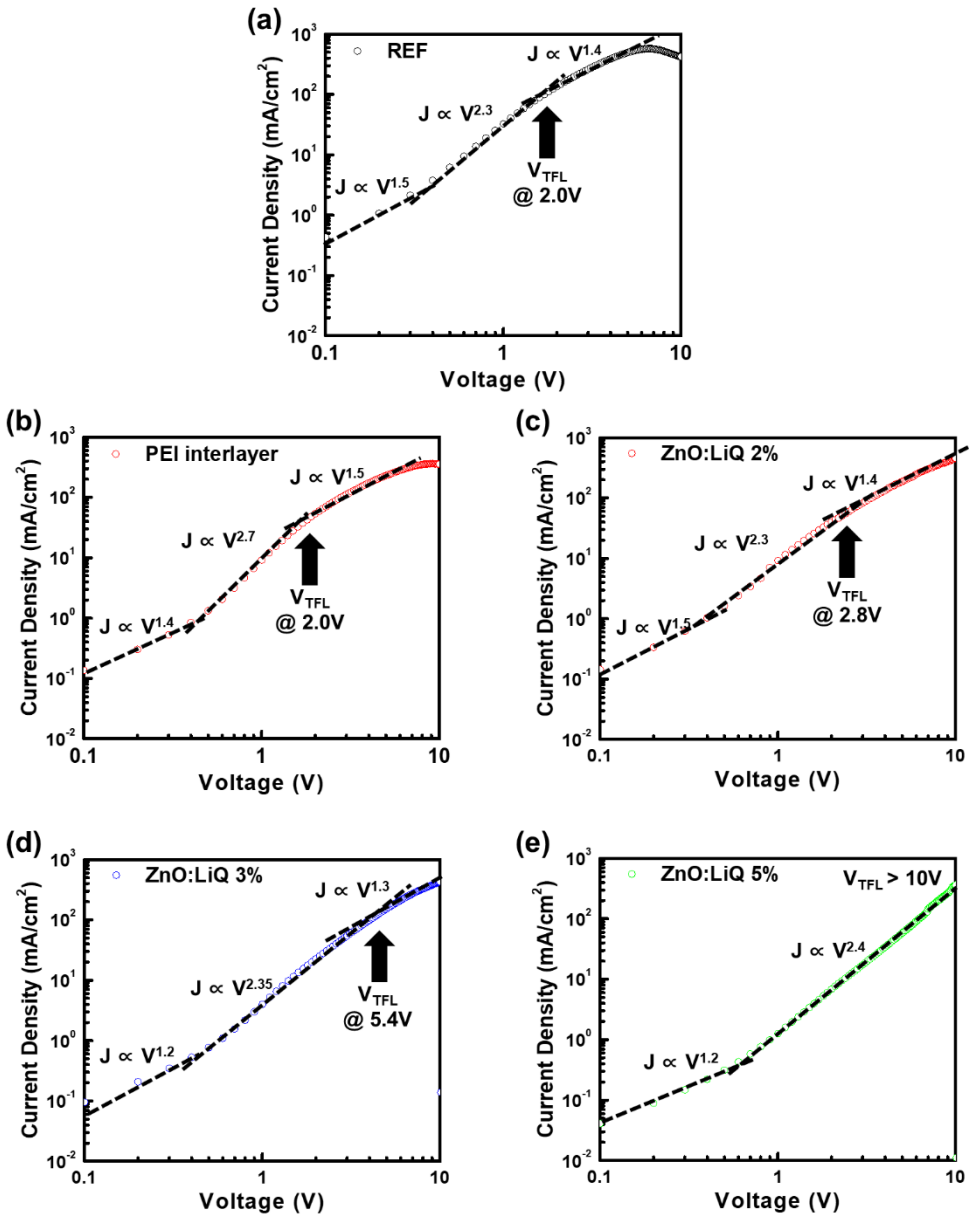

Figure 4.9. Current density-voltage (*J-V*) curve of EODs with (a) ZnO. (b) PEI/ZnO. (c) ZnO:LiQ 2%. (d) ZnO:LiQ 3%. and (e) ZnO:LiQ 5%.

Based on this analysis, we concluded that when a thin PEI interlayer is applied, the exciton quenching that occurs at the interface between the EML and ETL is suppressed to improve efficiency. However, since a very thin PEI interlayer is applied, the improvement in the characteristics is more noticeable in the low-field region, and we concluded that there was no improvement in the room-temperature operational lifetime. In the case of the ZnO:LiQ ETL, quenching at the interface between the EML and ETL is further enhanced, degrading efficiency. However, since it reduces the number of excess electrons injected into the EML, the room-temperature operational lifetime is improved. Therefore, we decided to combine the PEI interlayer, which improves the efficiency but does not enhance the lifetime, with the ZnO:LiQ ETL, which degrades the efficiency but improves the lifetime, in order to fabricate a device that improves the lifetime while maintaining the same level of efficiency.

4.2.3 PEI/ZnO:LiQ ETL

Figure 4.10 shows the results of evaluating the combination of the PEI interlayer and ZnO:LiQ ETL. Similar to the previous experimental results, the current efficiency improved by about 15% when the PEI interlayer was applied (6.37 cd/A → 7.33 cd/A). When the ZnO:LiQ ETL was combined, the efficiency declined. The device to which the PEI/ZnO:LiQ 5% condition was applied had an efficiency of 6.48 cd/A, which is similar to that of the reference device. However, because the interlayer that suppresses electron injection and the doped-ETL were applied together, the PEI/ZnO:LiQ 5% device was turned on at 2.5 V, whereas the reference device was turned on at 2.2 V. Although the current efficiency of the PEI/ZnO:LiQ 5% device was equivalent to that of the reference device, its power efficiency declined by 25% (5.72 lm/W → 4.32 lm/W).

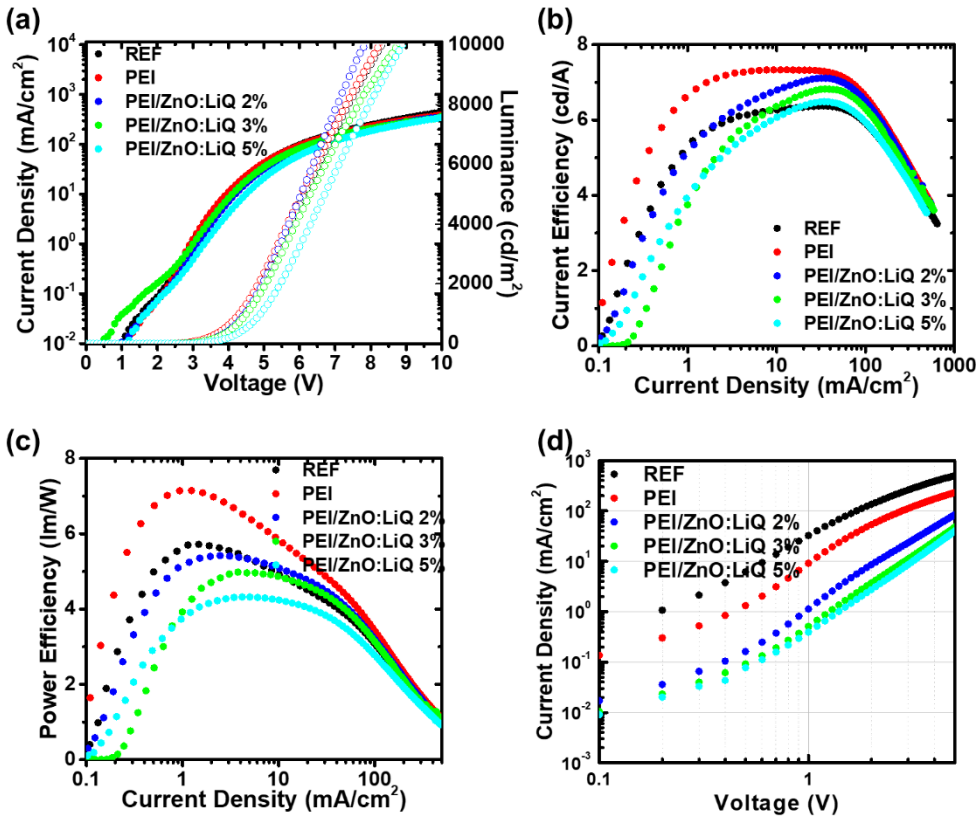

Figure 4.10. Electroluminescence (EL) performance of the QLEDs with combinations of PEI interlayer and ZnO:LiQ ETLs. (a) Current density-voltage-luminance (*J-V-L*) characteristics. (b) Current efficiency-current density characteristics. (c) Power efficiency-current density characteristics. (d) Current density-voltage (*J-V*) characteristics of EODs.

Device	V_{on} (V)	V_d (V)	Max CE (cd/A)	Max PE (lm/W)	λ_{max} (nm)	CIE coordinate (x,y)
Ref	2.2	4.4	6.37	5.72	627	(0.68, 0.32)
PEI	2.2	4.4	7.33	7.15	626	(0.68, 0.32)
PEI/ZnO:LiQ 2%	2.3	4.4	7.11	5.42	627	(0.68, 0.32)
PEI/ZnO:LiQ 3%	2.3	4.5	6.82	4.98	627	(0.68, 0.32)
PEI/ZnO:LiQ 5%	2.5	4.9	6.48	4.32	627	(0.68, 0.32)

[a] V_{on} is the turn-on voltage corresponding to 1 cd/m^2, and V_d is the driving voltage corresponding to 1000 cd/m^2.

Table 4.5. Performance summary of QLEDs with various ETLs.

Among various conditions, a comparative evaluation of the room-temperature operational lifetime was performed between the reference device and the device structure (PEI/ZnO:LiQ 5%) with the equivalent current efficiency. Similar to the earlier evaluation, the comparative evaluation of operational lifetime was conducted in a thermo-hygrostat chamber (25℃, 40%). The change in the luminance was observed while a constant current was operated at the current values that generated a luminance of 300 nits, 500 nits, and 1000 nits, respectively. According to **Fig. 4.11**, when the operational lifetime was evaluated at the luminance of 300 nits, T_{50} of the reference was 22 hours, while T_{50} of PEI/ZnO:LiQ was 51 hours. Hence, T_{50} increased by about 2.3 times. When the operational lifetime was evaluated at the luminance of 500 nits, T_{50} increased by about 2.6 times, from 10 hours to 26 hours. When the operational lifetime was evaluated at the luminance of 1000 nits, T_{50} increased by 2.5 times, from 4 hours to 10 hours. These results confirm that when the PEI/ZnO:LiQ ETL is applied, the operational lifetime improves by over two times while the same level of current efficiency is maintained.

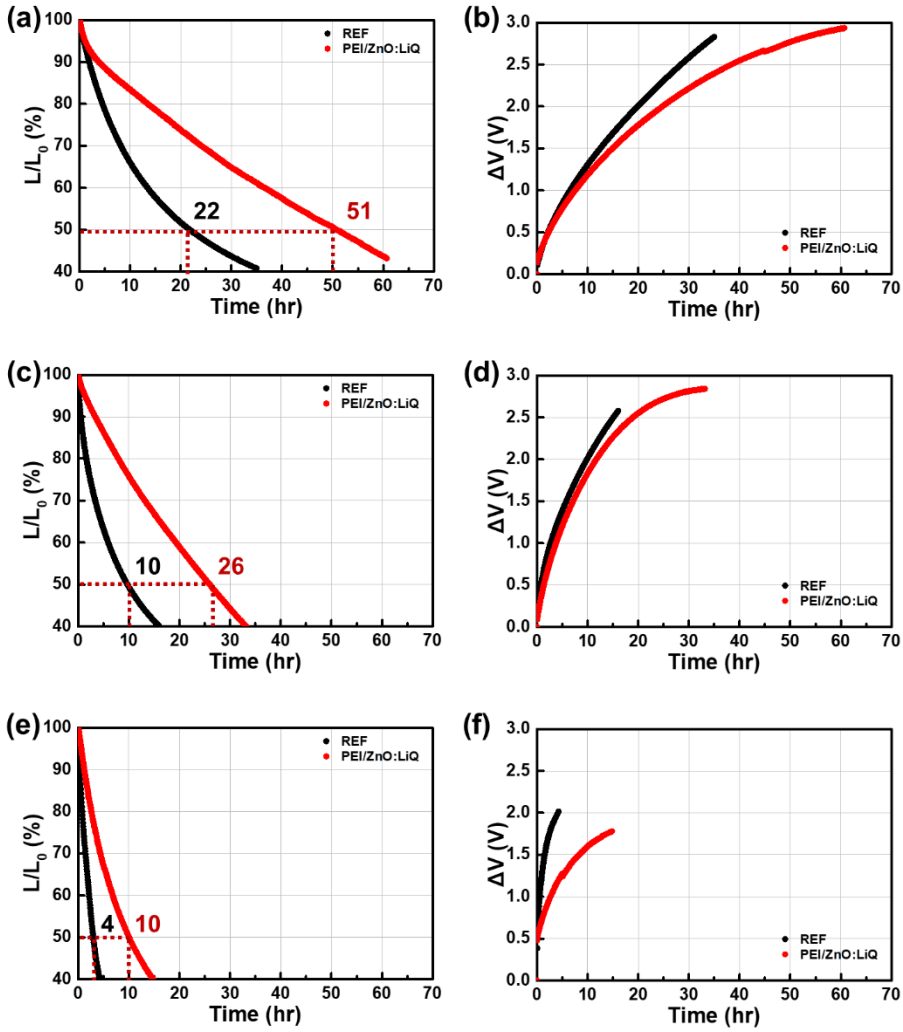

Figure 4.11. Luminance decay and driving voltage increase vs time of the QLEDs with combinations of PEI interlayer and ZnO:LiQ ETLs at different initial luminance. (a, b) 300 nit. (c, d) 500 nit and (e, f) 1000 nit.

The lifetime accelerator coefficient (n) was calculated based on the T_{50} evaluated above. n generally has a value between 1 and 2, and the smaller the value of n, the device operates robustly, even at high luminance. The equation used for the calculation is as follows [29, 33].

$$L_0^n \times LT_{50} = constant$$

As shown in **Fig. 4.12**, the accelerator coefficient of the reference device is 1.49, whereas the accelerator coefficient of the PEI/ZnO:LiQ device is 1.35. Hence, the value of n is smaller for the condition where electron injection is suppressed. Therefore, it is verified that when the PEI/ZnO:LiQ ETL structure is applied, the device has a more improved operational lifetime while maintaining a current efficiency equivalent to that of the reference device.

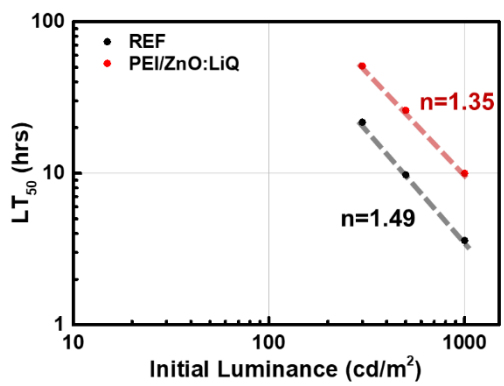

Figure 4.12. Measured LT_{50} values for different devices with operated at different initial luminance. The slope correspond to the accelerator coefficients.

4.3 Conclusion

In this study, we proposed a highly stable QLED device structure by incorporating a PEI interlayer and a monomer-doped ETL, LiQ, with ZnO. The application of the PEI interlayer resulted in a reduction in exciton quenching, leading to a 20% improvement in current efficiency. Conversely, no improvement in current efficiency or power efficiency was observed with the use of the LiQ-doped ETL; however, an enhanced operational lifetime was achieved due to the suppression of excess electrons resulting from a decrease in electron mobility. Ultimately, by combining these two approaches, we have developed a device structure that maintains an equivalent level of current efficiency while significantly improving operational lifetime. Therefore, we expect that the QLED devices produced through this simple approach will make a significant contribution to the large-area display market, such as TVs, where long lifetimes are required.

References

1. B. S. Mashford, M. Stevenson, Z. Popovic, C. Hamilton, Z. Zhou, C. Breen, J. Steckel, V. Bulovic, M. Bawendi, S. Coe-Sullivan, and P. T. Kazlas, "High-efficiency quantum-dot light-emitting devices with enhanced charge injection," *Nat. Photon.* **7**, 407–412 (2013).

2. W. K. Bae, Y.-S. Park, J. Lim, D. Lee, L. A. Padilha, H. McDaniel, I. Robel, C. Lee, J. M. Pietryga, and V. I. Klimov, "Controlling the influence of Auger recombination on the performance of quantum-dot light-emitting diodes," *Nat. Commun.* **4**, 2661 (2013).

3. W.-C. Chao, T.-H. Chiang, Y.-C. Liu, Z.-X. Huang, C.-C. Liao, C.-H. Chu, C.-H. Wang, H.-W. Tseng, W.-Y. Hung, and P.-T. Chou, "High efficiency green InP quantum dot light-emitting diodes by balancing electron and hole mobility," *Commun. Mater.* **2**, 96 (2021).

4. N. Kirkwood, B. Singh, and P. Mulvaney, "Enhancing Quantum Dot LED Efficiency by Tuning Electron Mobility in the ZnO Electron Transport Layer," *Adv. Mater. Interfaces* **3**, 1600868 (2016).

5. S. Wang, Y. Guo, D. Feng, L. Chen, Y. Fang, H. Shen, and Z. Du, "Bandgap tunable Zn 1−x Mg x O thin films as electron transport layers for high performance quantum dot light-emitting diodes," *J. Mater. Chem. C* **5**, 4724–4730 (2017).

6. Y. Lee, B. G. Jeong, H. Roh, J. Roh, J. Han, D. C. Lee, W. K. Bae, J.-Y. Kim, and C. Lee, "Enhanced Lifetime and Efficiency of Red Quantum Dot Light-Emitting Diodes with Y-Doped ZnO Sol-Gel Electron-Transport

Layers by Reducing Excess Electron Injection," *Adv. Quantum Technol*. **1**, 1700006 (2018).

7. Y. Sun, W. Wang, H. Zhang, Q. Su, J. Wei, P. Liu, S. Chen, and S. Zhang, "High-Performance Quantum Dot Light-Emitting Diodes Based on Al-Doped ZnO Nanoparticles Electron Transport Layer," *ACS Appl. Mater. Interfaces* **10**, 18902–18909 (2018).

8. D. Li, B. Kristal, Y. Wang, J. Feng, Z. Lu, G. Yu, Z. Chen, Y. Li, X. Li, and X. Xu, "Enhanced Efficiency of InP-Based Red Quantum Dot Light-Emitting Diodes," *ACS Appl. Mater. Interfaces* **11**, 34067–34075 (2019).

9. S.-K. Kim, H. Yang, and Y.-S. Kim, "Control of carrier injection and transport in quantum dot light emitting diodes (QLEDs) via modulating Schottky injection barrier and carrier mobility," *J. Appl. Phys.* **126**, 185702 (2019).

10. N. N. Mude, C. Y. Lee, K. J. Eun, R. Lampande, J. H, Kwon, “High Performance Red Cadmium-free Inverted Quantum Dot Light Emitting Diodes,” *SID Symp. Dig. Tech. Papers* **50(1)**, 1164-1167 (2019)..

11. W. Jiang and H. Chae, "Efficiency Enhancement of Tris(dimethylamino)-phosphine-Based Red Indium Phosphide Quantum-Dot Light-Emitting Diodes via Chlorine-Doped ZnMgO Electron Transport Layers," *J. Phys. Chem. C* **124**, 25221–25228 (2020).

12. H.-M. Kim, W. Jeong, J. H. Kim, and J. Jang, "Stability of Quantum-Dot Light Emitting Diodes with Alkali Metal Carbonates Blending in Mg Doped ZnO Electron Transport Layer," *Nanomaterials* **10**, 2423 (2020).

13. A. Alexandrov, M. Zvaigzne, D. Lypenko, I. Nabiev, and P. Samokhvalov, "Al-, Ga-, Mg-, or Li-doped zinc oxide nanoparticles as

electron transport layers for quantum dot light-emitting diodes," *Sci. Rep.* **10**, 7496 (2020).

14. B. Kim, D. Lee, B. Hwang, Y. Eun, M.-Y. Ha, and C. K. Kim, "High Performance Top-Emission Quantum Dot Light-Emitting Diodes with Mg-Doped ZnO Nanoparticles Used as an Electron Transport Layer," *J. Nanosci. Nanotechnol*. **21**, 3747–3752 (2021).

15. J. Jing, L. Lin, K. Yang, H. Hu, T. Guo, and F. Li, "Highly efficient inverted quantum dot light-emitting diodes employing sol-gel derived Li-doped ZnO as electron transport layer," *Org. Electron.* **103**, 106466 (2022).

16. X. Dai, Z. Zhang, Y. Jin, Y. Niu, H. Cao, X. Liang, L. Chen, J. Wang, and X. Peng, "Solution-processed, high-performance light-emitting diodes based on quantum dots," *Nature* **515**, 96–99 (2014).

17. H. H. Kim, S. Park, Y. Yi, D. I. Son, C. Park, D. K. Hwang, and W. K. Choi, "Inverted Quantum Dot Light Emitting Diodes using Polyethylenimine ethoxylated modified ZnO," *Sci. Rep.* **5**, 8968 (2015).

18. K. Ding, H. Chen, L. Fan, B. Wang, Z. Huang, S. Zhuang, B. Hu, and L. Wang, "Polyethylenimine Insulativity-Dominant Charge-Injection Balance for Highly Efficient Inverted Quantum Dot Light-Emitting Diodes," *ACS Appl. Mater. Interfaces* **9**, 20231–20238 (2017).

19. J. Yun, J. Kim, H.-K. Jang, K. J. Lee, J. H. Seo, B. J. Jung, G. Kim, and J. Kwak, "Controlling charge balance using non-conjugated polymer interlayer in quantum dot light-emitting diodes," *Org. Electron.* **50**, 82–86 (2017).

20. Y. Fu, W. Jiang, D. Kim, W. Lee, and H. Chae, "Highly Efficient and Fully Solution-Processed Inverted Light-Emitting Diodes with Charge Control Interlayers," *ACS Appl. Mater. Interfaces* **10**, 17295–17300 (2018).

21. T. Davidson-Hall and H. Aziz, "The role of polyethylenimine in enhancing the efficiency of quantum dot light-emitting devices," *Nanoscale* **10**, 2623–2631 (2018).

22. L. Wang, J. Lin, X. Liu, S. Cao, Y. Wang, J. Zhao, and B. Zou, "Mg-Doped ZnO Nanoparticle Films as the Interlayer between the ZnO Electron Transport Layer and InP Quantum Dot Layer for Light-Emitting Diodes," *J. Phys. Chem. C* **124**, 8758–8765 (2020).

23. N. N. Mude, Y. Khan, T. T. Thuy, B. Walker, and J. H. Kwon, "Stable ZnS Electron Transport Layer for High-Performance Inverted Cadmium-Free Quantum Dot Light-Emitting Diodes," *ACS Appl. Mater. Interfaces* **14**, 55925–55932 (2022).

24. S. Lee, C.-Y. Han, A. Hong, J. Kim, H. Yang, B. J. Jung, and J. Kwak, "Inverted quantum dot light-emitting diodes with defect-passivated ZnO as an electron transport layer," *Semicond. Sci. Technol.* **34**, 085002 (2019).

25. D. S. Chung, T. Davidson-Hall, H. Yu, F. Samaeifar, P. Chun, Q. Lyu, G. Cotella, and H. Aziz, "Significant enhancement in quantum-dot light emitting device stability via a ZnO:polyethylenimine mixture in the electron transport layer," *Nanoscale Adv.* **3**, 5900–5907 (2021).

26. Y. Yuan, X. Xue, T. Wang, X. Chi, R. Wang, and W. Ji, "Polyethylenimine modified sol-gel ZnO electron-transporting layers for quantum-dot light-emitting diodes," *Org. Electron.* **100**, 106393 (2022).

27. B. Liu, L. Lan, Y. Liu, H. Tao, H. Li, H. Xu, J. Zou, M. Xu, L. Wang, J. Peng, and Y. Cao, "Improved performance of quantum dot light-emitting diodes by hybrid electron transport layer comprised of ZnO nanoparticles doped organic small molecule," *Org. Electron.* **74**, 144–151 (2019).

28. S.-Y. Yoon, Y.-J. Lee, H. Yang, D.-Y. Jo, H.-M. Kim, Y. Kim, S. M. Park, S. Park, and H. Yang, "Performance Enhancement of InP Quantum Dot Light-Emitting Diodes via a Surface-Functionalized ZnMgO Electron Transport Layer," *ACS Energy Lett.* **7**, 2247–2255 (2022).

29. D. S. Chung, T. Davidson-Hall, G. Cotella, Q. Lyu, P. Chun, and H. Aziz, "Significant Lifetime Enhancement in QLEDs by Reducing Interfacial Charge Accumulation via Fluorine Incorporation in the ZnO Electron Transport Layer," *Nano-Micro Lett.* **14**, 212 (2022).

30. B. Y. Kim, S. J. Lee, J. R. Koo, S. E. Lee, K. H. Lee, J. A. Yoon, W. Y. Kim, S. S. Yoon, and Y. K. Kim, "Efficient Green Phosphorescent Organic Light-Emitting Diodes Depending on Concentration of Lithium Quinolate in Electron Transport Layer," *J. Nanosci. Nanotech.* **13**, 7998–8001 (2013).

31. J. Pan, J. Chen, Q. Huang, L. Wang, and W. Lei, "A highly efficient quantum dot light emitting diode via improving the carrier balance by modulating the hole transport," *RSC Adv.* **7**, 43366–43372 (2017).

32. J. H. Chang, P. Park, H. Jung, B. G. Jeong, D. Hahm, G. Nagamine, J. Ko, J. Cho, L. A. Padilha, D. C. Lee, C. Lee, K. Char, and W. K. Bae, "Unraveling the Origin of Operational Instability of Quantum Dot Based Light-Emitting Diodes," *ACS Nano* **12**, 10231–10239 (2018).

33. T. Doe, K. Kitano, S. Yamamoto, M. Yamamoto, K. Goto, Y. Sakakibara, T. Kobashi, H. Yamada, M. Ueda, T. Ryowa, M. Izumi, and Y. Arakawa, "Evaluation of degradation behavior in quantum dot light-emitting diode with different hole transport materials via transient electroluminescence," *Appl. Phys. Lett.* **118**, 203503 (2021).

Chapter 5

Summary, Limitations and Suggestions for Future Research

5.1 Summary

In this dissertation, we proposed two methods for improving the charge imbalance of conventional structure QLEDs fabricated via a solution process.

First, we proposed a device structure with improved hole injection by mixing monomers (TCTA or mCP) in the HTL. To improve the hole injection, we selected TCTA, a monomer with faster mobility than PVK, which was used as the reference, and mCP, which has a deep HOMO and can lower the injection barrier. We then mixed each monomer with PVK and applied them as the HTL. We also checked the electrical and optical properties of the device fabricated by controlling the device characteristics using a simple method of mixing monomers into the HTL. Unlike previous studies that focused on enhancing the hole injection, this study aimed to separately analyze the effect of the charge transport ability of HTL and the effect of the charge injection ability of HTL on the hole injection into the EML. In addition, we verified the effect of the material's intrinsic properties, such as T_g and energy level, on the device characteristics. Through this study, we proposed a development strategy for improving the luminous efficiency of QLEDs and decreasing the

driving voltage. Furthermore, we were able to develop an effective device structure.

Next, we developed a device structure that suppressed excess electrons being injected to improve the charge balance. We applied and evaluated PEI as an interlayer that functions as an injection barrier to electrons and LiQ to reduce the mobility of the ETL. The cause of changes in the efficiency was analyzed by observing the changes in the device behavior as the interlayer and LiQ doping were applied. In addition, the room-temperature operational lifetime was evaluated for each condition. When the PEI interlayer is applied, the efficiency of the device is improved by preventing the exciton quenching at the interface between the EML and ETL. It was also found that doping the ETL with the LiQ monomer reduces excess electrons and thus improves the operational lifetime of the device. Furthermore, by combining the interlayer and the doped ETL, we developed a device structure with an operational lifetime that has been improved by more than two-fold while maintaining the same level of efficiency. To further investigate the behavior of the device fabricated in this manner, we verified the device's characteristics in more detail by performing an SCLC analysis of the time-resolved PL and *J-V* curve. Through this study, we proposed a strategy for developing highly reliable QLEDs and verified a device structure with a long operational lifetime.

In conclusion, we have identified two different approaches for improving the characteristics of conventional QLEDs fabricated via the solution process. The two strategies for improving the charge imbalance showed different changes in the device characteristics: either the efficiency improved while the driving voltage decreased, or the reliability improved,

depending on the approach. Thus, we have verified that device characteristics can be optimized for various applications by appropriately controlling the device structure.

5.2 Limitations and Suggestions for Future Research

In this section, we discuss the limitations of our study and suggestions for researchers who will conduct follow-up studies. This discussion focuses on the analysis of mechanisms and strategies for improving device characteristics.

5.2.1 Factors Influencing the Operational Lifetime

In general, it is known that improving charge balance can have a significant impact on the stability and operation lifetime of the device. Similar to that, we also believed that the enhancement of hole injection through the reduction of electron-hole charge imbalance could lead to an improvement in operational lifetime. However, as shown in **Fig. 5.1**, indicating that the stability for PVK:TCTA 20% was at a similar level with reference, and no significant improvement in operational lifetime was observed with the enhancement of hole injection as expected.

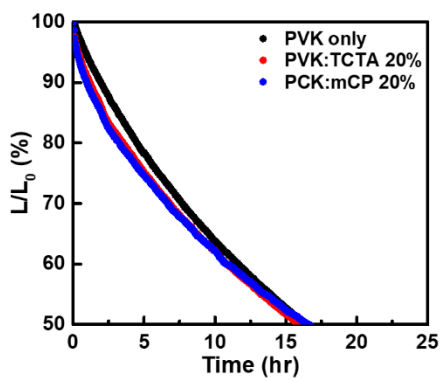

Figure 5.1. Luminance decay vs time of the QLEDs with different HTLs.

To investigate the reason for the lack of improvement in stability despite the improvement in charge balance, we analyzed research results that showed no improvement in operational lifetime despite the improvement in charge balance, not only in QLEDs, but also in OLEDs known to be electron-rich. Based on the searching of multiple research papers, several studies [1-3] have reported similar results, and in particular, the study by Kang et al. [3] focuses on analyzing the reasons for the decrease in lifetime despite the improvement of charge balance in OLEDs.

Upon reviewing several papers, we found that there are various factors that affecting the stability in addition to charge balance. To confirm the degree of charge imbalance between electrons and holes in our device, we additionally fabricated an EOD and compared it with HODs. As shown in **Fig. 5.2**, when comparing EOD with HODs, it was confirmed that hole injection was enhanced when mixing TCTA with PVK, but electron-rich conditions still persisted. Therefore, even if the degree of charge imbalance is alleviated, excess electrons were still present and could be the main cause of degradation in the device. We also considered the possibility that TCTA is more vulnerable to excess electrons, and that even if the amount of total excess electrons in the EML is reduced by mixing monomers, this may not lead to an improvement in operational lifetime.

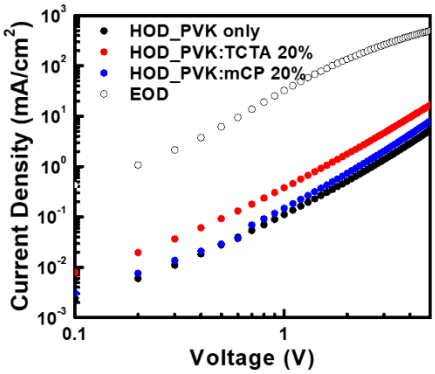

Figure 5.2. Current density-voltage (*J-V*) characteristics of the hole only devices with different HTLs and electron only device.

Unfortunately, the experiment we designed for enhancing hole injection did not improve the stability of the device, and we did not obtain a clear conclusion as to the cause for now. Factors affecting the stability of luminescent devices are diverse, and particularly, the operational lifetime of QLEDs is an interesting area that has not been extensively researched compared to OLEDs. Therefore, we propose further research on various factors that influence the operational lifetime of QLEDs. Through these researches, it is expected that we will be able to interpret the behavior of QLED devices more fundamentally. Furthermore, based on this understanding, we can take a leap forward in designing device structures and improving their characteristics.

5.2.2 Ultimate QLEDs with High Efficiency and Long Lifetime

In this study, we aimed to improve device characteristics through two different approaches: enhancing hole injection and improving charge balance by suppressing electron injection. When hole injection was enhanced, the carrier density, which affects the recombination rate, increased. As a result, the luminous efficiency improved, and the driving voltage decreased. Based on these characteristics, the hole injection enhanced QLEDs attained characteristics suitable for mobile-oriented applications, such as smartphones and smartwatches, which are powered by batteries and have a relatively short replacement cycle. In addition, when electron injection was suppressed, the luminous efficiency did not improve because the carrier density was reduced. However, device degradation due to excess electrons was prevented, thus improving the operational lifetime of the device. Therefore, characteristics were attained that are suitable for applications like TV, which are connected to a power source and have a relatively long replacement cycle.

Based on the results of each study, we thought that if the two methods were combined, it would optimize the charge imbalance and maximize the device characteristics. Accordingly, it may be possible to develop a device structure with high efficiency and a long lifetime that can be applied universally to various applications. Hence, we fabricated a device by combining hole injection enhancement and electron suppression and evaluated the device. **Figure 5.3** shows the evaluation results. The evaluation results show that compared to the reference device, the current efficiency of the HT-enhanced device increased by about 20%, and the power efficiency of the HT-enhanced device improved by 50%. On the other hand, in the ET-

suppressed condition, the current efficiency increased by about 5%, and the power efficiency improved by 10%.

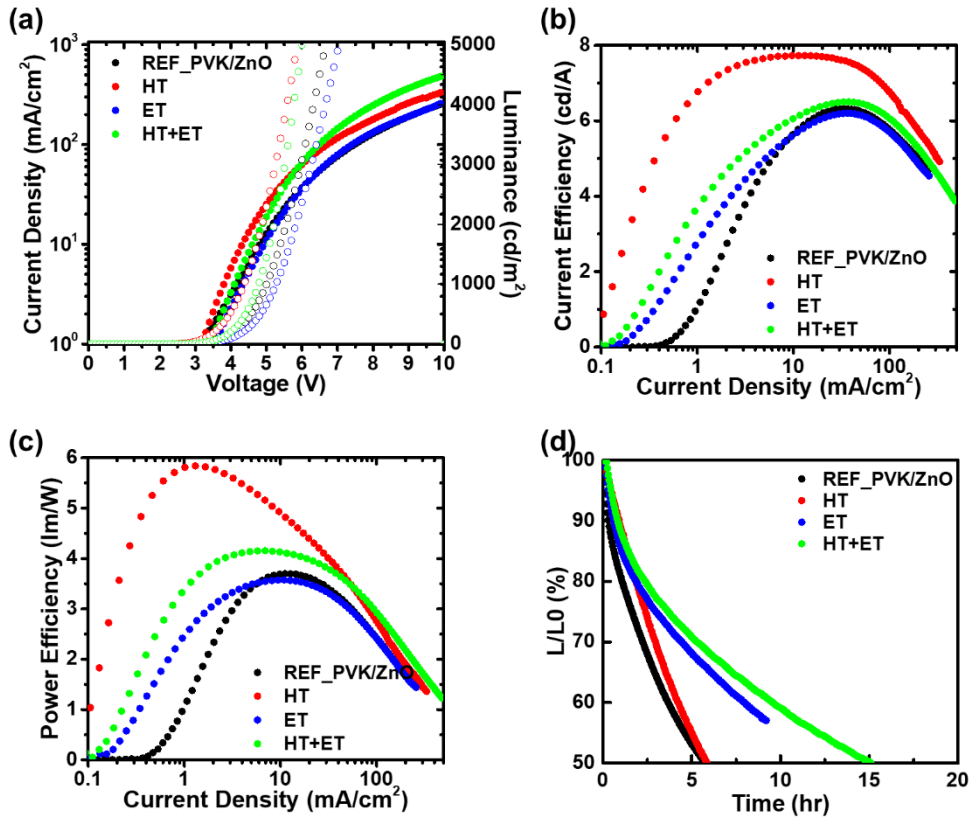

Figure 5.3. Electroluminescence (EL) performance of the QLEDs with combinations of PVK:TCTA 20% (HT) and PEI/ZnO:LiQ ETL (ET). (a) Current density-voltage-luminance (*J-V-L*) characteristics. (b) Current efficiency-current density characteristics. (c) Power efficiency-current density characteristics. (d) Luminance decay vs time.

Device	V_{on} (V)	V_d (V)	Max CE (cd/A)	Max PE (lm/W)	λ_{max} (nm)	CIE coordinate (x,y)
Ref_PVK/ZnO	2.5	5.0	6.32	3.70	627	(0.68, 0.32)
HT (PVK:TCTA)	2.2	4.3	7.73	5.84	627	(0.68, 0.32)
ET (PEI/ZnO:LiQ)	2.6	5.2	6.20	3.57	628	(0.68, 0.32)
HT+ET	2.5	4.7	6.50	4.16	627	(0.68, 0.32)

[a] V_{on} is the turn-on voltage corresponding to 1 cd/m^2, and V_d is the driving voltage corresponding to 1000 cd/m^2.

Table 5.1. Performance summary of QLEDs with various ETLs.

To understand why the margin of characteristic improvement is different between the two approaches, the HOD and EOD for each condition are shown together in **Fig. 5.4**. When comparing the EOD and HOD in the reference condition, the current density of the EOD is significantly larger than that of the HOD. Hence, the charge imbalance is very large. Therefore, it seems that in the reference condition with many excess electrons, recombination of exciton were likely to occur actively as hole injection was enhanced. On the other hand, if we look at the EOD of the condition where electron injection is suppressed, the current density is very low. Therefore, the degree of charge imbalance has already been reduced as the number of excess electrons decreased. Hence, it seems that the likelihood of improving exciton recombination by enhancing hole injection was relatively low.

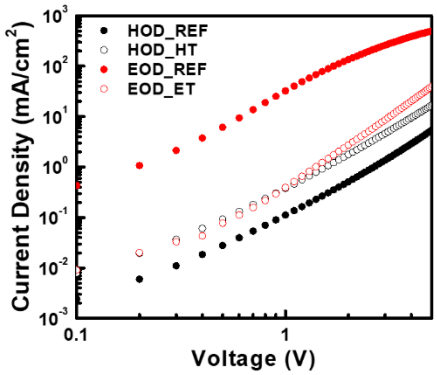

Figure 5.4. Current density-voltage (*J-V*) characteristics of the hole only devices with different HTLs and electron only devices with different ETLs.

Unfortunately, a powerful device that exhibits all of the following characteristics, high efficiency, low power consumption, and long lifetime, could not be developed in this study. However, when the two methods of improving the charge balance are compared, the method of enhancing hole injection, which causes recombination to occur actively to improve the device characteristics, is more advantageous. Therefore, follow-up studies should be conducted to develop device structures that can enhance hole injection and operate robustly even in the presence of excess electron attacks. Through further studies, it is expected that QLEDs with further improved characteristics will be widely used in the display industry.

References

1. J. H. Hwang, J. Kim, B. J. Kim, M. Park, Y. W. Kwon, M. An, D. Y. Shin, J. M. Jeon, J. Y. Kim, W. Lee, J. Lim, and D. Lee, "Hole injection of quantum dot light-emitting diodes facilitated by multilayered hole transport layer," *Appl. Surf. Sci.* **558**, 149944 (2021).

2. T. Doe, K. Kitano, S. Yamamoto, M. Yamamoto, K. Goto, Y. Sakakibara, T. Kobashi, H. Yamada, M. Ueda, T. Ryowa, M. Izumi, and Y. Arakawa, "Evaluation of degradation behavior in quantum dot light-emitting diode with different hole transport materials via transient electroluminescence," *Appl. Phys. Lett.* **118**, 203503 (2021).

3. S. Kang, J. Y. Lee, and T. Kim, "Unveiling the Root Cause of the Efficiency-Lifetime Trade-Off in Blue Fluorescent Organic Light-Emitting Diodes," *Electron. Mater. Lett.* **16**, 1–8 (2020).

Appendix

Publication List

International Journal

1. **Y. Kim**, H. Park, J. Yoon, H. Yoon, S. Jeong, D. Kim and Y. Hong*, “Monomer-mixed Hole Transport Layers for Improving Hole Injection of Quantum Dot Light-emitting Diodes”, *Optics Express* **31**, 20730 (2023).

International/Domestic Conferences

1. **Y. Kim**, H. Yoon, G. Kim, S. Jeong, J. Yoon, D. Kim and Y. Hong*, " Improvement of Efficiency Roll-off in Red Quantum-dot Light Emitting Diodes by Controlling Electron Injection", The 21st International Meeting on Information Display 2021 (IMID 2021), Seoul/Online, Korea, August (2021) (Poster)
2. **Y. Kim**, H. Yoon, G. Kim, S. Jeong, J. Yoon, D. Kim and Y. Hong*, Optimizing Charge Balance of Quantum-Dot Light Emitting Diodes via Controlling Hole/Electron Injection", 2022 Materials Research Society (MRS) Spring Meeting & Exhibit, Honolulu, USA, May (2022) (Poster)
3. J. Park, J. Yoon, **Y. Kim**, Y. Hong*, " Selective Coating CdSe/ZnS Quantum Dots on Stretchable Substrate with Controlled Density by Inducing Ligand Exchange Reaction", SID Display Week 2022, San Jose, USA, May (2022) (poster)

국문 초록

디스플레이의 응용처가 더욱 다양화, 고도화 됨에 따라 다양한 수요를 만족시키기 위하여 관련 기술들이 계속하여 발전하고 있다. CRT, LCD 와 같이 후면 발광체를 필수 요소로 하는 디스플레이의 시대를 지나 LED, OLED 와 같은 자체발광 소자를 기반으로 하는 디스플레이가 시장을 석권하고 있다. 특히 최근 디스플레이 분야의 차세대 주자로 주목받고 있는 소재로는 양자점과 페로브스카이트 등을 꼽을 수 있다. 이 중 양자점은 전기적, 광학적으로 우수한 성질을 가지고 있어 발광 소자 및 센서 등과 같은 제품에 다양하게 활용이 가능한 반도체성 물질이다. 입자 크기 제어를 통해 발광/흡수 파장의 조절이 용이하고, 높은 색 순도와 고 휘도를 구현할 수 있으며 코어-쉘/리간드의 제어를 통해 특성을 다양하게 조절할 수 있다는 장점이 있다. 또한 용매에 분산된 형태로 공정에 활용할 수 있기 때문에 용액 공정을 통해 저비용/저온 공정이 가능하여 대면적의 유연/신축성 전자 소자로의 응용을 기대할 수 있어 더욱 주목받고 있다.

양자점 발광 다이오드를 가장 쉽고 효율적으로 제작하기 위한 방법으로 알려진 것은 회전판에 장착한 기판 위에 용액을 떨어뜨린 후, 회전을 통한 원심력을 활용하여 박막을 증착 하는 “스핀 코팅(Spin-Coating)”이다. 스핀 코팅은 공정이 간단하고,

코팅 속도가 빠르며 비교적 균일한 막 두께를 확보할 수 있다. 뿐만 아니라 회전판의 회전 속도, 회전 시간 및 용액의 농도 등으로 박막의 두께를 용이하게 조절할 수 있다는 장점이 있다.

그러나 이렇게 제작된 양자점 발광 소자에는 본질적인 특성의 한계점이 존재하는데, 이는 양자점의 최대 가전자대 (VBM, valence band maximum)에 기인하는 전하 불균형 상태이다. 양자점은 깊은 최대 가전자대를 갖기 때문에 발광층으로의 정공 주입 장벽이 전자 주입 장벽 대비하여 크게 형성된다. 뿐만 아니라 용액 공정으로 활용 가능한 정공 수송층의 정공 이동도는 전자 수송층의 전자 이동도 대비 매우 낮은 것으로 알려져 있다. 따라서 주입 장벽과 전하의 이동도라는 두 가지 측면 모두에서 정공의 주입이 전자 주입 대비 불리하고, 이에 따라 과잉 전자가 다수 존재하는 전하 불균형 상태가 된다. 이러한 전하 불균형은 비발광재결합을 야기하여 소자 특성을 저하시키는 주요한 원인이 된다. 따라서, 본 논문에서는 이러한 문제점들을 해결하기 위하여 다양한 소자 구조 개발 전략을 제시하고자 하였다.

우선 기능층의 추가 없이 단량체를 정공추입층에 혼합하여 사용하는 소자 구조를 제안하였다. 정공 주입을 개선하기 위하여 증착 공정을 통해 정공 주입층을 성막 하는 역구조의 양자점 발광 다이오드와 달리, 단량체의 혼합을 통해 정공 이동도와 주입 장벽을 제어하면서도 기존의 구조와 공정을 유지할 수 있다는 장점을 갖는다. 이러한 소자 구조 개발을 위하여 적절한 물성을 갖는 단량체의 탐색과, 용해도 및 용매 직교성에 대한 사전

평가가 수반되었다. 이를 통해 간단한 공정을 유지하면서 정공 주입을 효과적으로 강화하여 소자의 광학적, 전기적 특성을 크게 개선할 수 있었다.

다음으로는 과잉 전자를 억제할 수 있는 소자 구조를 개발하고자 하였다. 이러한 소자 개발을 위하여 과잉 전자 억제를 위해서 전자 주입 장벽을 추가하는 방법과, 전자수송층의 전자이동도를 제어하는 두 가지 방법이 모두 평가되었다. 뿐만 아니라 과잉 전자를 제어함에 따라 소자의 거동이 변화하는 원리를 규명하고자 하였다. 이러한 연구를 통하여 전하 불균형 상태를 완화할 수 있었으며 이에 따라 높은 신뢰성을 갖는 소자 구조를 확보할 수 있었다.

본 학위논문은 다양한 단량체를 용액 공정에 적용할 수 있는 공정 기술을 개발하고, 양자점 발광 다이오드의 성능을 향상시킬 수 있는 기반 기술을 개발하는데 그 목적을 두었다. 특히 다양한 단량체의 물성을 적절하게 활용하여 양자점 발광 다이오드의 특성을 그 필요에 따라 최적화 하고자 하였다. 이에 따라 저전력, 고효율 또는 고안정성을 확보하기 위한 양자점 발광 다이오드의 개발 전략을 제시하였으며 결과적으로 디스플레이 산업에 QLED 가 활용될 수 있는 기반 기술 개발에 큰 기여를 할 수 있을 것으로 기대한다.

주요어: 용액 공정, 양자점, 양자점 발광 다이오드, 단량체, 전하 균형

학번: 2019-30461